Molecular Plant
Research Article

CellPress
PARTNER JOURNAL

Quantitative Trait Loci Analysis Identifies a Prominent Gene Involved in the Production of Fatty Acid-Derived Flavor Volatiles in Tomato

Karolina Garbowicz[1,6], Zhongyuan Liu[2,6], Saleh Alseekh[1,3,6], Denise Tieman[2], Mark Taylor[2], Anastasiya Kuhalskaya[4], Itai Ofner[5], Dani Zamir[5], Harry J. Klee[2], Alisdair R. Fernie[1,3] and Yariv Brotman[4,*]

[1]Max-Planck-Institute of Molecular Plant Physiology, Potsdam-Golm, Germany

[2]Horticultural Sciences, Plant Innovation Center, University of Florida, Gainesville, FL, USA

[3]Center of Plant System Biology and Biotechnology, 4000 Plovdiv, Bulgaria

[4]Department of Life Sciences, Ben-Gurion University of the Negev, Beersheba, Israel

[5]Robert H. Smith Institute of Plant Sciences and Genetics, Faculty of Agriculture, Hebrew University of Jerusalem, Rehovot 7610001, Israel

[6]These authors contributed equally to this article.

***Correspondence: Yariv Brotman (brotman@mpimp-golm.mpg.de)**

https://doi.org/10.1016/j.molp.2018.06.003

ABSTRACT

To gain insight into the genetic regulation of lipid metabolism in tomato, we conducted metabolic trait loci (mQTL) analysis following the lipidomic profiling of fruit pericarp and leaf tissue of the *Solanum pennellii* introgression lines (IL). To enhance mapping resolution for selected fruit-specific mQTL, we profiled the lipids in a subset of independently derived *S. pennellii* backcross inbred lines, as well as in a near-isogenic sub-IL population. We identified a putative lecithin:cholesterol acyltransferase that controls the levels of several lipids, and two members of the class III lipase family, *LIP1* and *LIP2*, that were associated with decreased levels of diacylglycerols (DAGs) and triacylglycerols (TAGs). Lipases of this class cleave fatty acids from the glycerol backbone of acylglycerols. The released fatty acids serve as precursors of flavor volatiles. We show that *LIP1* expression correlates with fatty acid-derived volatile levels. We further confirm the function of LIP1 in TAG and DAG breakdown and volatile synthesis using transgenic plants. Taken together, our study extensively characterized the genetic architecture of lipophilic compounds in tomato and demonstrated at molecular level that release of free fatty acids from the glycerol backbone can have a major impact on downstream volatile synthesis.

Key words: lipidomics, lipids, lipase, volatile, FA-VOC, *Z*-4-decenal

Garbowicz K., Liu Z., Alseekh S., Tieman D., Taylor M., Kuhalskaya A., Ofner I., Zamir D., Klee H.J., Fernie A.R., and Brotman Y. (2018). Quantitative Trait Loci Analysis Identifies a Prominent Gene Involved in the Production of Fatty Acid-Derived Flavor Volatiles in Tomato. Mol. Plant. **11**, 1147–1165.

INTRODUCTION

Tomato is one of the most widely grown crops in the world, being both versatile and rich in nutrients, vitamins, and antioxidants. The tomato clade (*Solanum* sect. *Lycopersicon*) consists of 13 recognized wild species (Peralta et al., 2006), with *Solanum pennellii* considered one of the most distant relatives of the cultivated tomato (*Solanum lycopersicum*). This small desert species, bearing green fruits, has evolved unique adaptations to thrive in arid habitats, and as it is sexually compatible with *S. lycopersicum* it was used as the founding donor parent of a well-characterized *S. pennellii* introgression line (IL) population (Eshed and Zamir, 1995). The ILs, representing whole-genome coverage of *S. pennellii*, have contributed over the years to the identification of genes responsible for diverse traits including pathogen resistance (Martin et al., 1993), fruit ripening (Manning et al., 2006), sodium and potassium homeostasis (Asins et al., 2013), whole plant morphology and yield (Ronen et al., 2000; Lippman et al., 2007; Alseekh et al., 2013), and fruit morphology and size (Frary et al., 2000; Liu et al., 2002; Xiao et al., 2008), as well as having considerably aided in our understanding of the genetic regulation of primary and secondary metabolism.

Published by the Molecular Plant Shanghai Editorial Office in association with Cell Press, an imprint of Elsevier Inc., on behalf of CSPB and IPPE, SIBS, CAS.

Metabolite levels can be regarded as a quantitative traits, and mapping them using structured populations facilitates the identification of the genomic regions associated with the metabolic variation—so-called metabolic quantitative trait loci (mQTLs). In this manner novel metabolic and regulatory genes have been identified in a range of different plant species (Kliebenstein et al., 2002; Chan et al., 2011; Li et al., 2013; Chen et al., 2014; Matsuda et al., 2015; Wu et al., 2018). In tomato, using the *S. pennellii* ILs, this approach was successfully utilized for primary metabolites (Causse et al., 2004; Overy et al., 2005; Schauer et al., 2008; Toubiana et al., 2012, 2015), secondary metabolites (Rousseaux et al., 2005; Tieman et al., 2006a; Minutolo et al., 2013; Alseekh et al., 2015, 2017; Schilmiller et al., 2015, 2016), and volatile organic compounds from tomato fruit (Mathieu et al., 2009; Mageroy et al., 2012; Rambla et al., 2014, 2017). However, relatively few studies to date have been aimed at understanding the genetic basis of lipid composition in tomato populations, and most of the performed studies have targeted cuticular lipids in fruits and leaves (Yeats et al., 2012; Bolger et al., 2014; Ofner et al., 2016; Fernandez-Moreno et al., 2017). Studying wax triterpenoid composition, Yeats et al. (2012) shed new light on understanding the ecological and evolutionary functional genomics of plant cuticles. In addition, the first screening for a large set of cuticular lipids in tomato fruit using *S. pennellii* ILs was performed by Fernandez-Moreno et al. (2017) in order to build a first map of associated QTLs. Targeted analysis with this population has also been carried out on the lipophilic carotenoids (Ronen et al., 2000) and tocopherol (Quadrana et al., 2014). Overall, very little has been achieved thus far in understanding the genetics underlying the metabolism and regulation of lipids, a class of compounds with prominent roles in practically every aspect of life (Tenenboim and Brotman, 2016; Nakamura, 2017).

Lipids and fatty acids serve as precursors for many volatile compounds that contribute to defense, signaling, and, in the case of fruits, the attraction of herbivores and consequent seed distribution (Wang et al., 2001; Chen et al., 2004; Klee and Giovannoni, 2011). One of the main defense hormones, jasmonic acid, involved in induced systemic resistance and in response to wounding, is derived from linolenic acid (Vick and Zimmerman, 1984). Fatty acids were shown to directly induce the expression of defense-associated *R* genes (Chandra-Shekara et al., 2007). Plant fatty acid-derived volatile organic compounds (FA-VOCs) have critical functions in many aspects of intra- and inter-kingdom communication (Weber, 2002). They are specifically induced in response to many biotic stresses such as pathogen and herbivore feeding, where they have important defensive functions (Dicke and Baldwin, 2010; Christensen and Kolomiets, 2011; Scala et al., 2013). In addition, many FA-VOCs are important contributors to human liking of food crops (Schwab et al., 2008; Tieman et al., 2017). In the case of tomato, several FA-VOCs, including multiple C5, C6, C7, C8, and C10 volatiles, are significantly correlated with overall liking and flavor intensity (Tieman et al., 2017). Even within the species *S. lycopersicum*, there is tremendous variation in FA-VOC content; levels of these chemicals within ripe fruit can vary by several orders of magnitude (Tieman et al., 2017). Knowledge of how these volatiles are synthesized and how their biosynthetic pathways are regulated is critical for the development of varieties with superior flavor in ways that do not compromise plant defense.

Given the importance of these chemicals in plant defense and agronomic quality, there are large gaps in our understanding of FA-VOC biosynthetic pathways. For example, the roles of lipoxygenases (LOX) and hydroperoxide lyase (HPL) in the later steps of the pathway are well established in synthesis of C5 and C6 volatiles (Vancanneyt et al., 2001; Chen et al., 2004; Shen et al., 2014). While LOX activity is essential for synthesis of these volatiles, there is little evidence that LOX isoforms are rate limiting to synthesis. Although it is theoretically logical to assume that release of polyunsaturated fatty acids from the glycerol backbone of mono-, di-, and triglycerides would be an essential first step to synthesis of any FA-VOC, there is a critical lack of knowledge concerning this first step. Moreover, virtually nothing is known about synthesis of longer-chain FA-VOCs such as *Z*-4-decenal and *E*,*E*-2,4-decadienal, two volatiles that are significantly correlated with liking tomato flavor. Cleavage of fatty acids from glycerol is accomplished by the action of lipases. Genes predicted to encode lipases are abundant in plant genomes and have been implicated in multiple biological processes. For example, several class III lipases have critical roles in mobilizing stored lipids during seed germination (Eastmond, 2004a, 2004b; Matsui et al., 2004), while others respond to stresses or senescence (Jakab et al., 2003; Ling, 2008). Moreover, the Defective in Anther Dehiscence 1 protein (DAD1), an *Arabidopsis* lipase, catalyzes the initial step of jasmonic acid biosynthesis (Ishiguro et al., 2001).

Here, we conducted large-scale lipid profiling of fruit pericarp and leaf material of an *S. pennellii* IL population. We detected 1528 fruit and 428 leaf mQTLs, and identified many candidate genes in the process. We selected three loci and used independently derived *S. pennellii* backcrossed inbred lines (BILs), as well as an independent near-isogenic sub-IL population, for fine-mapping. We revealed three candidate genes that associated with the abundance of lipids, a putative lecithin:cholesterol acyltransferase and two members of the class III lipase gene family, *LIP1* and *LIP2*, all of which are highly expressed in *S. pennellii*. We generated *LIP1* overexpression and RNAi-mediated knockdown lines and confirmed a role for LIP1 in reduced lipid and increased glycerol and FA-VOC contents in the *S. pennellii*-derived IL12-3 that harbors the *LIP1* gene. Our study provided an extensive analysis of the genetic architecture of tomato lipid metabolism, showed a critical role of a lipase gene in the regulation of FA-VOC synthesis, and identified an allele likely positively affecting tomato fruit volatiles that are significantly correlated with consumer preferences.

RESULTS

LC–MS-Based Lipidomic Profiling of *S. pennellii* Introgression Lines

To explore the genetic basis of lipid metabolism in tomato, we performed lipidomic analysis using ultra-performance liquid chromatography coupled with Fourier-transform mass spectrometry (UPLC-FT-MS) on fruit pericarp and leaf tissue from a population of 76 ILs derived from a cross between *S. pennellii* and *S. lycopersicum* (M82). Fruit pericarp tissue

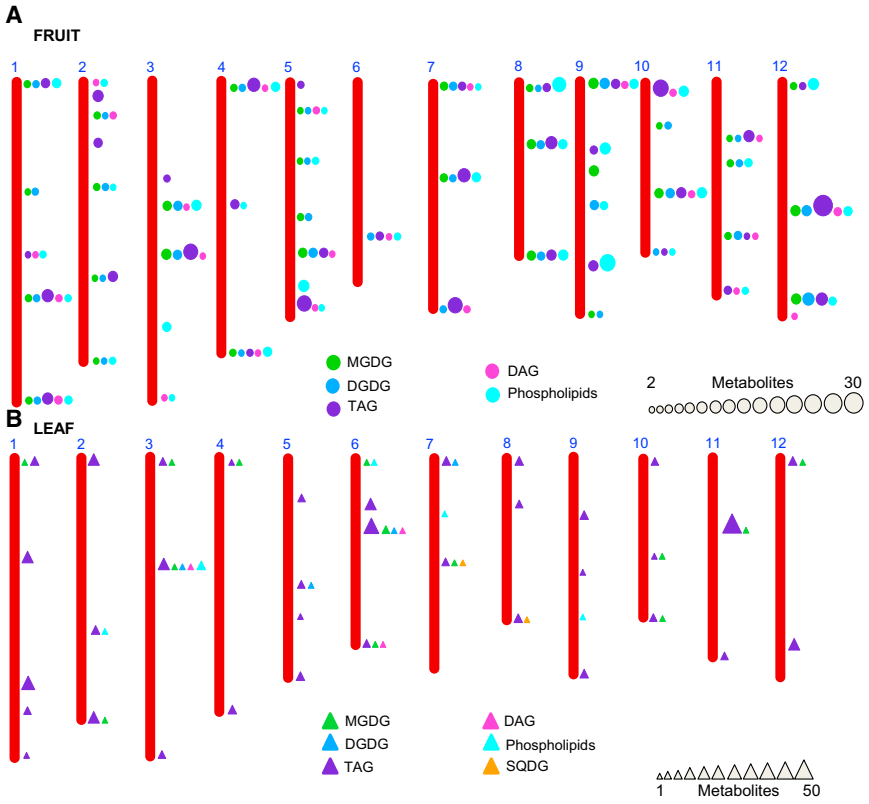

Figure 1. Summary of Mapping Results Conducted in Fruit and Leaf

Chromosomal distribution of the mQTL found in the IL mapping of ripe fruit **(A)** and leaf **(B)** tissue. For fruit, lipid–locus associations that were present in the two harvesting seasons ($p < 0.05$; 2001 and 2003) are shown. Leaf lipid–locus associations ($p < 0.001$) in which IL lipid levels were either more than 3-fold or less than 0.5-fold of the M82 value are shown. Each circle (triangle) represents an mQTL, color-coded according to lipid class, and its size represents the number of lipid species participating in a given mQTL.

was harvested in two independent field trials (2001 and 2003 summer seasons, Israel; previously described in Schauer et al., 2006), whereas leaf material was obtained from ILs grown in the greenhouse in the spring of 2016. The following lipid classes were measured: phosphatidylcholines (PCs), phosphatidylethanolamines (PEs), phosphatidylglycerols (PGs), phosphatidylinositols (PIs), phosphatidylserines (PSs), diacylglycerols (DAGs), triacylglycerols (TAGs), monogalactosyldiacylglycerols (MGDGs), digalactosyldiacylglycerols (DGDGs), and sulfoquinovosyl diacylglycerols (SQDGs).

The two parental strains show profound differences between their lipophilic compound profiles, both in fruit and leaf, with differences in almost every lipid class (Supplemental Figure 1A and 1B). Strikingly, *S. pennellii* ripe fruit contains substantial amounts of lipophilic compounds that are absent in M82. In fruit, we identified 135 and 163 lipid species in the 2001 and 2003 harvest seasons (Table S1), respectively, of which 117 lipid species (belonging to five classes: PCs, PEs, DAGs, TAGs, MGDGs, and DGDGs) were common to both seasons (Supplemental Table 1). Lipid levels reached a maximum of nearly 45-fold-chnage compared with M82, with around 43% and 57% of all detected changes in lipids showing increased or decreased levels in the ILs, respectively, in comparison with M82.

Using the same strategy, we investigated lipid metabolism in the leaf. This allowed us to identify 203 lipid species across all ILs (Supplemental Table 1). In contrast to fruit pericarp, in the leaf we observed major changes in TAG contents, with most of the ILs showing increases in TAGs when compared with M82 (Supplemental Figure 2A and 2B). Interestingly, only two ILs show a significant decrease in the leaf level of these compounds.

Identification of Lipid QTLs in the *S. pennellii* IL Population

Next, lipid QTLs were defined using ANOVA performed at two levels of significance: permissive ($p \leq 0.05$) and stringent ($p \leq 0.01$). We found a total of 1528 and 738 mQTLs with the permissive and stringent threshold, respectively, in fruit across two seasons. In leaf 428 associations at $p \leq 0.001$ were identified (Supplemental Table 2). Conserved mQTLs (with permissive threshold) across two seasons in fruit, and robust mQTLs in leaf ($p \leq 0.001$), were plotted next to the genome segment to which they were mapped (Figure 1A and 1B). While mostly evenly distributed across the genome, several hotspots were identified, notably on chromosome 3 (IL3-3), 5 (IL5-3, IL5-4), 8 (IL8-2), 9 (IL9-2, IL9-3), and 12 (IL12-2, IL12-3, IL12-4) in fruit; and in leaf on chromosome 1 (IL1-3, IL1-4), 3 (IL3-3), 6 (IL6-1, IL6-2, IL6-2-2), 11 (IL11-2), and 12 (IL12-4).

To further investigate the effect of introgression of the wild allele in the genetic background of the domesticated tomato, we explored the distribution of detected QTLs for each lipid class across all ILs (Supplemental Figure 3A and 3B). In fruit, 14 ILs showed, in parallel, substantial increase and decrease in lipid content (see, for instance, ILs 3-2/3-3/5-3/5-4), while 12 ILs displayed only decreased lipid levels (see, for instance, ILs 7-1/7-2/12-2/12-4). Lipid levels in the rest of the ILs exhibited mixed behavior, but still showed a general tendency to change in one direction (Supplemental Figure 3A). In leaf, the ILs manifested a smaller degree of variation in lipid abundance (Supplemental Figure 2), mostly confined to increased TAG levels in the majority of the lines (Supplemental Figure 3B).

Conducting lipid mapping in both tissues allowed us to identify tissue-specific QTLs and to reveal different genetic regulation of lipid metabolism in fruit and leaf. In fruit around 56.6% of detected mQTLs were associated with decreased lipid levels, whereas in leaf most of the changes contributed to TAG

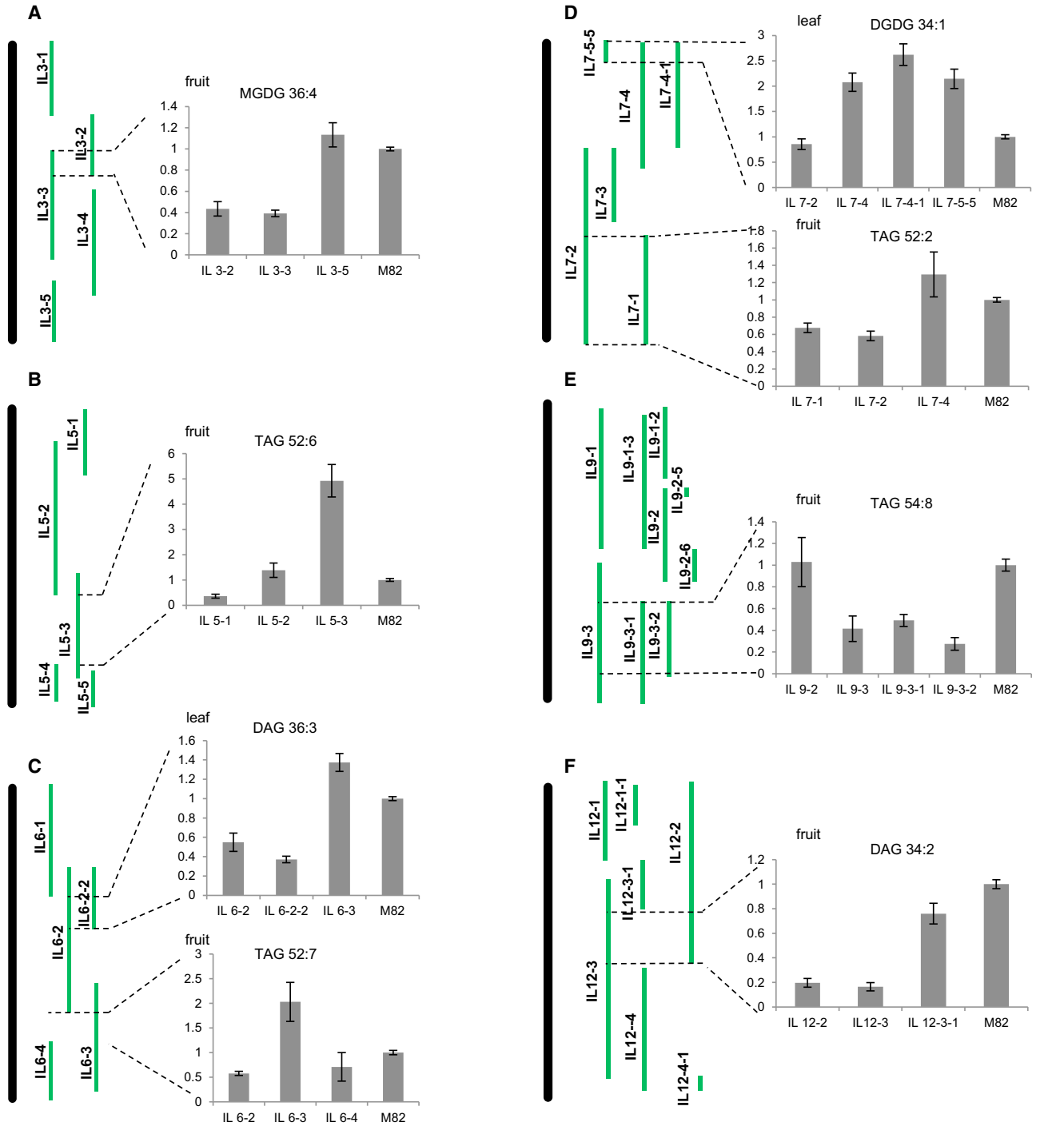

Figure 2. Schematic Representation of *S. pennellii* ILs for Six Chromosomes in Fruit and Leaf.

Representative lipid species are depicted (A–F), showing the effect of genomic regions on lipid levels. Only significant mQTLs are shown ($p < 0.05$). Lipid levels were calculated as fold change of M82. Error bars indicate SE. $n = 8$ for fruit, $n = 4$ for leaf.

accumulation. For example in ILs 12-2/IL12-3 (Supplemental Figure 3A), we detected a major fruit-specific metabolic quantitative trait locus (mQTL) that led to lower levels of mostly TAGs and DAGs. Conversely, a strong mQTL that influenced the levels of different lipid classes in both tissues is located in the wild genomic segment carried by IL3-3.

Our lipid profiling revealed that lines carrying overlapping introgressed genomic segments show, in many cases, a similar lipid profile (Supplemental Figure 3 and Figure 2), enabling us to narrow down the genomic region of the QTL. For instance, levels of MGDG 36:4 are altered by a gene(s) in an overlapping region of IL3-2 and IL3-3 (Figure 2A), whereas chromosome 6

may contain genes involved in diacylglycerol and triacylgycerol metabolism (Figure 2C). Additionally, almost 37% of all TAGs displayed significantly lower levels in ILs that carry a 19-cM segment of chromosome 9 (Figure 2E) common to IL9-3, IL9-3-1, and IL9-3-2.

Identification of Candidate Genes

To identify causal genes within the intervals corresponding to the identified mQTLs, we used the genetic markers that define the ends of the overlapping region of each IL to identify the genomic sequence in the assembly of tomato genome available at the Sol Genomics Network (assembly ITAG3.1; http://solgenomics.net). Next, we generated a list of tomato genes putatively annotated, based on sequence homology, as lipid metabolism-related. We then searched publicly available expression data (TFGD, http://ted.bti.cornell.edu/) for lipid-related genes located in the mQTL hotspots and extracted those that were differentially expressed between the two parental lines (Table 1). In segment IL1-1, for instance, we identified 30 lipid-related genes, two of which were differentially expressed between M82 and *S. pennellii*: *Solyc01g008780*, encoding a putative phospholipase A2; and *Solyc01g008320*, encoding a protein that contains a DDHD domain, which is commonly observed in phosphoesterases. In another mQTL, located in the overlap region of IL8-2 and IL8-2-1, we identified a gene (*Solyc08g066800*) that shows strong sequence homology to phospholipase D, an enzyme that uses PC, PE, and PG as substrates. Indeed, not only were increased levels of PC and PE associated ($p < 0.01$) with this locus, but also expression of *Solyc08g066800* in IL8-2 and IL8-2-1 was low compared with M82, implicating it as the causal gene. *Solyc03g097470*, predicted to encode β-ketoacyl-acyl carrier protein synthase III that takes part in *de novo* fatty acid biosynthesis in the chloroplast, is highly expressed in *S. pennellii* and located in an mQTL on IL3-3. This mQTL is associated with altered levels of various lipid classes, mainly decreased TAG levels. Interestingly, the M82 allele contains an 8-bp deletion 816 bp from the transcriptional start site, as well as several changes within the first 50 bp upstream of the transcriptional start site when compared with the *S. pennellii* allele, changes that might be causal for the altered gene expression.

mQTL Validation in IL5-3 Using an *S. pennellii* Backcross Inbred Lines Population

Our QTL analysis revealed that the introgressed region of IL5-3 on chromosome five significantly altered the levels of several lipids, mostly triacylglycerols (Figure 3A). Based on sequence homology, this region contains 25 lipid-related genes, 13 of which are expressed in fruits. To gain better mapping resolution, we performed lipid analysis on fruit pericarp material of a subset of independently derived *S. pennellii* BILs (Ofner et al., 2016; Figure 3B). From the collection of ~446 BILs available we selected 49 BILs that contain an introgression overlapping with that of IL5-3. The lipidomic profiling revealed that 9 out of 49 BILs showed similar phenotype to IL5-3 (Figure 3C). Based on the overlap of the nine *S. pennellii*-like BILs, we defined a much-reduced interval containing 12 genes, among which only one (*Solyc05g050710*, lecithin:cholesterol acyltransferase) was annotated to have a putative function in lipid metabolism. This gene additionally shows 20-fold higher expression in *S. pennellii* and in IL5-3 compared with M82 (Figure 3D). Moreover, we found that the basis for the differential expression might lie in a 43-bp deletion in the promoter region of the M82 allele of the gene (Figure 3E).

A Major mQTL on Chromosome 12 Regulates the Levels of TAGs and DAGs in Tomato Fruit

A major fruit-specific mQTL for DAGs and TAGs (0.0179 relative level of M82) was detected in the overlapping regions of IL12-2 and 12-3 when compared with M82 in tomato fruit pericarp (Figures 1A and 2F). This region contains 859 genes, including 15 annotated as lipid-related. To obtain better mapping resolution, we selected eight BILs that contain introgressions of *S. pennellii* that overlap with that of IL12-2/12-3. Lipid profiling of those lines revealed four BILs with similarly decreased TAG and DAG levels as IL12-2/12-3 (Figure 4A and Supplemental Table 3). Based on the overlap of the *S. pennellii*-like BILs we defined a much-reduced interval of 100 genes, among them four lipid-related. To further narrow down the locus we generated a series of sub-ILs derived from the cross of IL12-3 to M82 (Figure 4B). Sites of recombination within these sub-ILs were defined by the markers listed in Supplemental Table 4. By comparing the lipid content of each sub-IL to M82, we identified a segment of *S. pennellii* controlling contents of the TAG and DAG classes. The border of this segment was defined by molecular markers C36605 and S459-2. All sub-ILs containing this segment had substantially lower levels of DAGs and TAGs compared with M82 (Figure 4C), while those sub-ILs without this segment were unchanged or higher than M82. Annotation of the tomato genome (Tomato Genome Consortium, 2012) indicates the presence of approximately 60 genes within this interval (Supplemental Table 5). The transcript levels of those genes that are involved in lipid metabolism in ILs and the parental lines revealed that only *Solyc12g055730*, putatively annotated as a class III triacylglycerol lipase, was highly abundant in fruits of IL12-2 and 12-3 (RNA-sequencing data [TFGD, http://ted.bti.cornell.edu/]; Figure 4D), and not in leaves, which concomitantly showed an opposite trend in lipid levels. We named this lipase *LIPASE1* (*SlLIP1* for the M82 allele and *SpLIP1* for the *S. pennellii* allele). Triacylglycerol lipases are enzymes capable of hydrolyzing ester linkages of triglycerides and diglycerides, releasing a free fatty acid (Mukherjee, 1994). This action corresponds to the lower levels ($p < 0.01$) of TAGs and DAGs observed in the IL12-2 and IL12-3. Although there are 27 amino acid differences between the SpLIP1 and SlLIP1 enzymes, they both contain the lipase consensus sequence FVVTGHSLGG and the SDH catalytic triad (Supplemental Figure 4A). DNA sequencing of the orthologous promoter regions revealed a 1307-bp insertion into the *SlLIP1* gene, moving a tandem repeat of primary ethylene response elements (PEREs) substantially further away from the translational start site (Supplemental Figure 4B). PERE elements have been shown to confer ethylene-inducible gene expression in *Arabidopsis* (Solano et al., 1998) and tobacco (Kosugi and Ohashi, 2000). These results tentatively suggest that LIP1 is likely to be a lipase catalyzing the release of fatty acids from triacylglycerols.

The Class III Lipase Family in Tomato

Class III lipases constitute a large family of lipolytic enzymes that degrade triacylglycerol into glycerol and free fatty acids. Analysis

mQTL	IL name	Gene name	Annotation	Expression		Fold change
				M82	*S. pennellii*	
MGDG, DGDG, TAG, Phospholipids	IL1-1	*Solyc01g008780*	Phospholipase A	**65.47**	27.01	2.4
MGDG, DGDG, TAG, Phospholipids	IL1-1	*Solyc01g008320*	DDHD domain	**91.77**	31.57	2.9
MGDG, DGDG, TAG, DAG, Phospholipids	IL1-3	*Solyc01g099040*	GDSL esterase/lipase	48.8	**3181.45**	65.2
MGDG, DGDG, TAG, DAG, Phospholipids	IL1-3	*Solyc01g099100*	Long-chain fatty acid coenzyme A ligase	**196.2**	52.47	3.7
MGDG, DGDG, TAG, DAG, Phospholipids	IL1-4/ IL1-4-8	*Solyc01g111250*	Phosphatidylinositol-specific phospholipase C	35.51	**205.89**	5.8
MGDG, DGDG, phospholipids	IL2-3/ IL2-4	*Solyc02g069420*	Phospholipid-translocating P-type ATPase flippase family protein	**51.07**	5.71	8.9
MGDG, DGDG, phospholipids	IL2-3/ IL2-4	*Solyc02g069430*	Phospholipid-transporting ATPase	**109.56**	9.32	11.8
MGDG, DGDG, phospholipids	IL2-3/ IL2-4	*Solyc02g069930*	Lipase-like protein	**154.25**	2.39	64.5
DAGs, DGDG, MGDG, TAG	IL3-3	*Solyc03g097470*	3-Oxoacyl-β-ketoacyl-acyl carrier protein synthase III (FabH)	143.29	**865.25**	6.0
DAGs, DGDG, MGDG, TAG	IL3-3	*Solyc03g111550*	GDSL esterase/lipase	**159.57**	1.74	91.7
DAGs, phospholipids	IL3-5	*Solyc03g123750*	Lipase (LIP2)	6.15	**34.59**	5.6
MGDG, DGDG, TAGs, DAGs	IL5-3	*Solyc05g050710*	Lecithin cholesterol acyltransferase	0.97	**50.05**	51.6
MGDG, DGDG, TAG, DAG, Phospholipids	IL6-2/ IL6-2-2	*Solyc06g054550*	Lipase	**61.26**	0	
MGDG, DGDG, TAG, DAG, Phospholipids	IL6-2/ IL6-2-2	*Solyc06g054670*	Stearoyl-acyl carrier protein desaturase	0	**64.55**	
MGDG, DGDG, TAG, DAG, Phospholipids	IL6-2/ IL6-2-2	*Solyc06g059710*	Stearoyl-acyl carrier protein desaturase	0	**55.76**	
MGDG, DGDG, TAG, DAG, Phospholipids	IL6-2/ IL6-2-2	*Solyc06g059720*	Stearoyl-acyl carrier protein desaturase	141.81	**3116.16**	22.0
MGDG, DGDG, TAGs, DAGs, phospholipids	IL7-4/ IL7-4-1	*Solyc07g019670*	Fatty acid oxidation complex subunit alpha	60.91	**593.51**	9.7
MGDG, DGDG, TAGs, phospholipids	IL8-2/ IL8-2-1	*Solyc08g066800*	Phospholipase D	**112.63**	9.35	12.0
DGDG, MGDG,TAGs, phospholipids	IL9-2	*Solyc09g020190*	Phosphoesterase	**64.33**	14.43	4.5
DGDG, phospholipids	IL9-3	*Solyc09g091050*	Lipase	**121.31**	12.28	9.9
TAGs, DAGs, phospholipids	IL10-1	*Solyc10g008640*	Diacylglycerol kinase	**62.65**	20.15	3.1
TAGs, DAGs, phospholipids	IL10-1	*Solyc10g075070*	Non-specific lipid-transfer protein	48.76	**7473.24**	153.3
TAGs, DAGs	IL12-2/IL12-3	*Solyc12g055730*	Lipase (LIP1)	2.44	**1582.28**	648.5

Table 1. Lipid-Related Genes Located in mQTL Hotspots.

of the tomato genome (Tomato Genome Consortium, 2012) identified seven pairs of lipase genes, *Sp/SlLIP1* to *Sp/SlLIP7*. The phylogenetic relationship between Sp/SlLIP1 and other lipases present in the tomato genome and their homologs in other plant species was charted (Figure 4E). Sp/SlLIP1 belongs to the same subgroup as RcOBL1 and EgLIP1. RcOBL1 is a

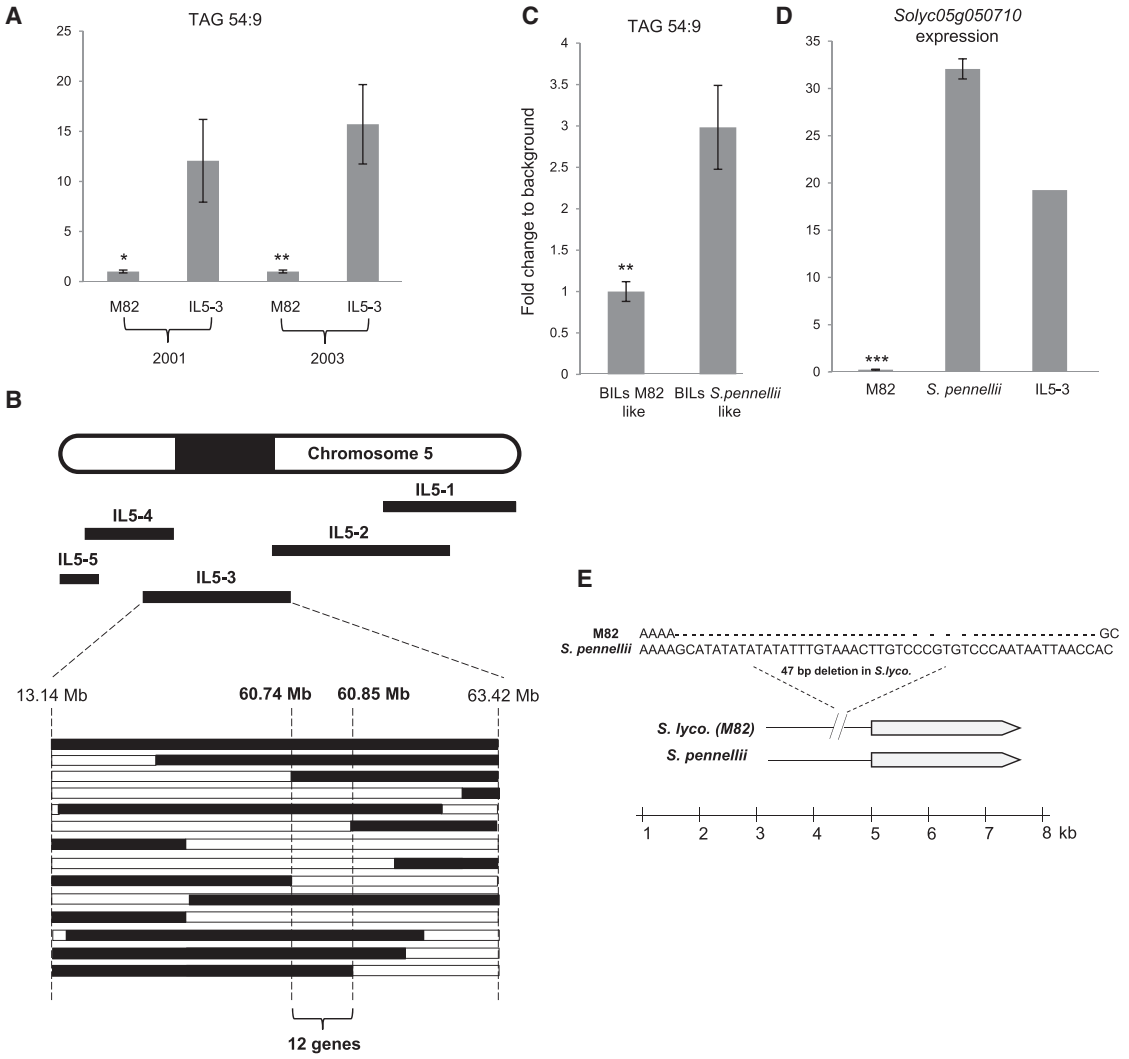

Figure 3. Fine-Mapping of an mQTL.

(A) Levels of TAG 54:9 in M82 and IL5-3 from two independent harvest seasons, showing one of the strongest differences in the entire mapping. Asterisks indicate significant differences (* $p < 0.05$, ** $p < 0.01$).

(B) Schematic representation of fine-mapping of IL5-3 using backcross inbred lines (BILs; bars below). Black bars represent *S. pennellii* introgression and white bars correspond to the M82 background. Interval borders are based on SNP location. The introgressed region of IL5-3 contains 25 lipid-related genes.

(C) Levels of TAG 54:9 in 11 BILs that share the *S. pennellii* segment in the spanning region compared with 40 BILs that have the M82 background in the same region. Asterisks indicate significant differences (** $p < 0.01$).

(D) Expression of *Solyc05g050710* in fruit of M82, *S. pennellii*, and IL5-3. Asterisks indicate significant differences ($p < 0.001$).

(E) The promoter of the M82 allele of *Solyc05g050710* features a 47-bp deletion compared with the *S. pennellii* allele.

class III lipase isolated from castor bean endosperm that hydrolyzes a range of triacylglycerols but is not active on phospholipids (Eastmond, 2004a). EgLIP1 was reported to be an oil palm class III lipase (Nurniwalis et al., 2015). qPCR analysis was performed to assess expression of the seven lipases in fruit of IL12–3 and M82. Of the seven, only SpLIP1 was highly expressed in ripe fruits, with expression 50-fold higher than in any of the other genes (Figure 4D).

Decreased DAGs and TAGs Are Associated with the *LIP2* Locus

Hierarchical clustering analysis on our lipid data from fruit pericarp revealed that IL3-5 grouped together and showed similar phenotypic pattern to IL12-2/12-3, with lower levels of DAGs and TAGs in fruits and no alteration in leaf (Figure 5A). The introgressed region of IL3-5 contains 425 genes, among them 20 lipid-related. Following the same strategy as described above, we conducted lipidomic analysis on a subset of 27 BILs overlapping with the introgression of *S. pennellii* in IL3-5, which revealed that 12 lines showed similar TAG and DAG levels as IL3-5 (Figure 5B). This permitted us to reduce the mQTLs to a genomic region containing 121 genes, five of which are putatively associated with lipid metabolism. Notably, *Solyc03g123750* (named *SlLIP2* for M82 allele and *SpLIP2* for *S. pennellii* allele), putatively annotated as a class III TAG lipase, is the only gene in this locus that showed differential mRNA accumulation, with 2.5-fold higher transcript in IL3-5 fruit

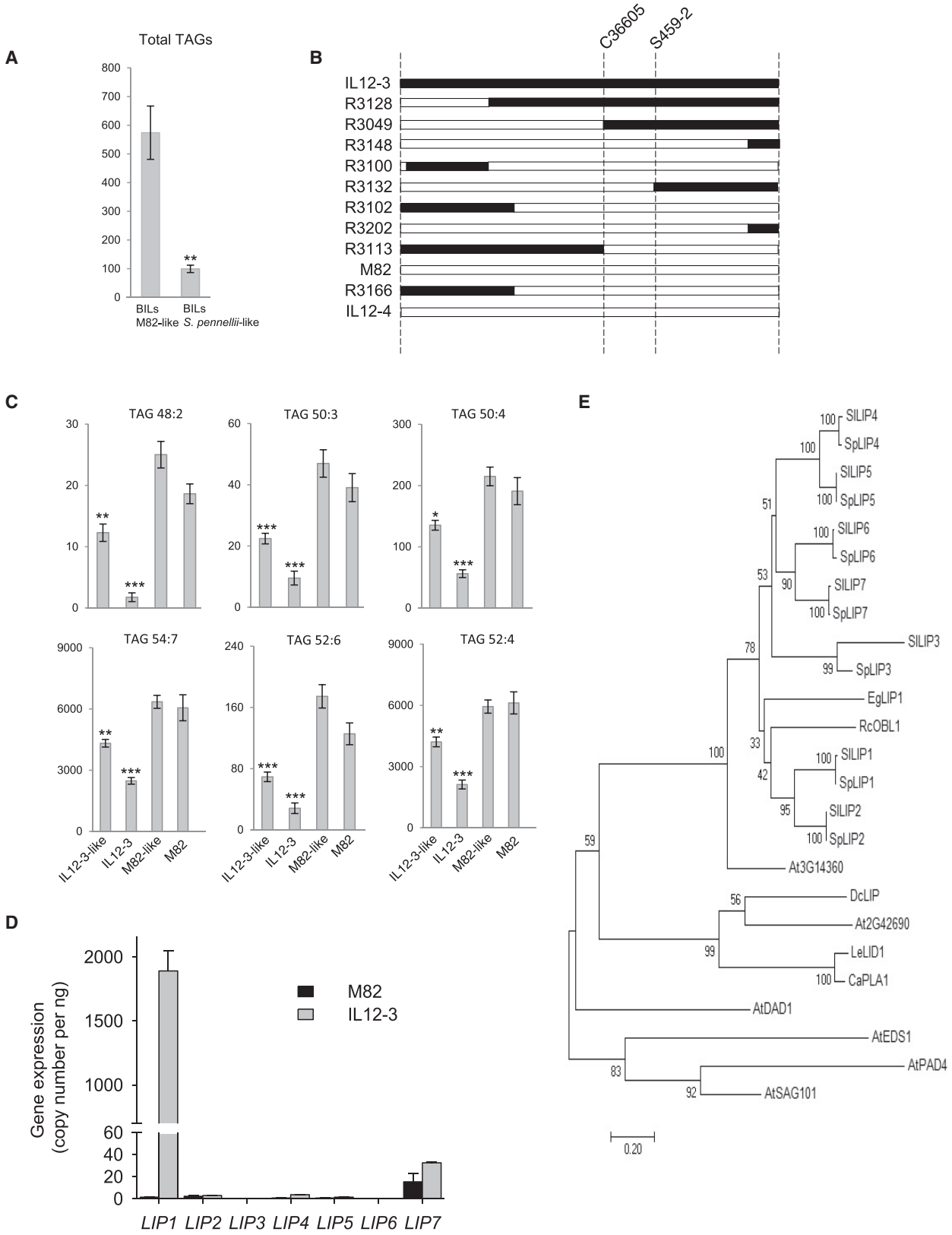

Figure 4. Characterization of the IL12-3 mQTL Harboring the *SlLIP1* Gene.

(A) Levels of total TAGs in M82-like BILs compared with *S. pennellii*-like BILs. The means of five (M82) and four (*S. pennellii*) lines are shown. Error bars indicate SE; asterisks indicate significant differences ($p < 0.05$).

(legend continued on next page)

compared with M82 (Figure 5C). Examination of the promoter region of *SlLIP2* and *SpLIP2* revealed a 38-bp and a 48-bp deletion in the M82 allele (Figure 5D). Sequence analysis revealed that the protein sequence of SlLIP1 has 62% identity and 73% similarity to SlLIP2. Despite some amino acid differences between the SlLIP1 and SlLIP2 enzymes, especially near the N terminus, they both contain the lipase-specific features as described above. Moreover, the phylogenetic analysis described above (Figures 4D or 5D) showed that SpLIP2 is the closest homolog of SpLIP1.

A QTL Associated with IL12-3 Regulates FA-VOC Production in Tomato Fruit

We have associated the decreased levels of DAG and TAG with a locus within IL12-3 containing the *LIP1*. Previously, we also showed that the *S. pennellii* introgression, IL12-3, produces significantly higher levels of multiple FA-VOCs (Tieman et al., 2006b). To better establish the effects of the introgression on volatile production, we grew IL12-3 for seven seasons and quantified a set of C5–C10 volatiles synthesized in fruit, several of which make significant contributions to consumer liking of tomato fruit (Tieman et al., 2017) (Supplemental Table 6). Among 15 FA-VOCs of different carbon chain length, six exhibited consistently higher levels in IL12-3 fruits over all the seasons, including 1-penten-3-one (C5), pentanal (C5), *E*-2-pentenal (C5), *E*-2-heptenal (C7), *Z*-4-decenal (C10), and *E*,*E*-2,4-decadienal (C10) with 1.5- to 18-fold increases in IL12-3. Other FA-VOCs, such as 1-pentanol, were significantly different in multiple but not all seasons. Based on these observations, IL12-3 contains one or more QTLs regulating the production of a range of FA-VOCs in fruit.

In addition, we performed FA-VOC analysis on the IL12-3 sub-IL population. The emissions of six FA-VOCs with higher levels in IL12-3 fruit were quantified in each sub-IL (Figure 6A). By comparing the FA-VOC emissions of each sub-IL to M82, we identified a segment (between markers C36605 and S459-2s) of *S. pennellii* controlling contents of the two C10 volatiles, *Z*-4-decenal and *E*,*E*-2,4-decadienal. This segment is identical to the one found by lipid mapping harboring the *LIP1*. All sub-ILs containing this segment had a substantially higher level of *Z*-4-decenal compared with M82 while those sub-ILs without this segment were unchanged or lower (R3148) than M82. For *E*,*E*-2,4-decadienal, five of the seven sub-ILs containing this segment emitted substantially higher levels than M82. However, no clear linkage with the other four FA-VOCs was observed with this genome region (Supplemental Table 10A).

Correlation between *SpLIP1* Expression and C10 FA-VOC Emission in IL12-3 Plants

Real-time RT–PCR analysis of *Sp/SlLIP1* expression in different tissues demonstrated that the *SpLIP1* transcript specifically accumulates in fruit tissue from the mature green to red ripe stage. While *SlLIP1* also accumulates to its highest levels in ripening fruit, *SpLIP1* is present in vastly higher levels at all stages of ripening (Figure 6B). Correspondingly, emissions of *Z*-4-decenal (Figure 6C) and *E*,*E*-2,4-decadienal (Figure 6D) increase at the turning stage and reach their highest levels at the red ripe stage in IL12-3 fruit, with significantly lower levels of these C10 volatiles in M82 than IL12-3. The positive correlation between *SpLIP1* transcript abundance and emissions of C10 FA-VOCs is consistent with a rate-limiting role for SpLIP1 in C10 FA-VOC production.

Functional Validation of *SpLIP1* Using Overexpression and RNAi Lines

To further validate the mapping results and the function of *LIP1 in vivo*, we introduced an RNAi construct into IL12-3, which resulted in multiple lines with up to 95% reduced expression of *SpLIP1* (Figure 7A). Expression of the other six lipases was also assessed (Supplemental Figure 5). *LIP4* was the only gene with reduced expression levels in all four independent RNAi lines. This reduction is not unexpected given its homology to *LIP1*. However, given the incredibly low expression levels of *LIP4* compared with *SpLIP1* in IL12-3 (Supplemental Figure 5), the contribution of off-target silencing of *LIP4* to the changes in the lipid levels observed in RNAi lines is likely to be negligible. In addition, we generated four independent overexpression (OE) lines carrying the *S. pennellii* allele (*SpLIP1*) driven by the figwort mosaic virus 35S promoter in the M82 background (Supplemental Figure 6). Lipid levels in red ripe fruit of four independent OE lines and four independent *LIP1*-downregulated RNAi lines were profiled. The OE lines show clear reduction in the levels of most lipid species, especially in DAGs and TAGs. These changes, therefore, resemble the lipid profile we observed in IL12-3, for example TAG 60:7 and TAG 58:7 (Supplemental Figure 6B and Supplemental Table 7). In contrast, downregulation of *LIP1* in the IL12-3 background restored DAGs to M82 levels, and increased TAG content to above M82 levels (Figure 7B and Supplemental Table 7). The most prominent changes were observed in the levels of TAG 52:6, TAG 50:6, and TAG 54:9, which were all significantly decreased in IL12-3 compared with M82 but substantially increased, following *SpLIP1* silencing, to levels well above those

(B) Fine-mapping of the chromosomal region using a sub-IL population. Each F4 generation sub-IL is shown by a combination of black and white rectangles, representing the *S. pennellii* and *S. lycopersicum* genome fragments, respectively. Sub-IL borders were defined with the molecular markers listed in Supplemental Table 1. The *SLIP1* gene lies between the two indicated markers.

(C) Levels of various representative TAGs in M82, IL12-3, and in sub-ILs that either harbor *SLIP1* (12-3-like) or not (M82-like) presented in relative values. Error bars indicate SE; asterisks indicate significant differences ($p < 0.05$).

(D) Expression levels of the seven *LIP*s in ripe fruit of IL12-3 and M82 (error bars represent SE, $n = 4$).

(E) Phylogenetic analysis of the protein sequences of the seven LIPs in *S. lycopersicum* and *S. pennellii*, as well as of homologs in other species. An unrooted neighbor-joining tree was generated by MEGA5.1. The percentage of trees in which the associated taxa are clustered together is shown next to the branches. The trees are drawn to scale, with branch lengths measured in the number of substitutions per site. GenBank accessions or NCBI reference numbers are as follows: SpLIP1 (XP_015060008), SlLIP1 (XP_004252623), At3G14360 (NM_112294.5), RcOBL1 (JQ945176), EgLIP1 (JX556215), AtDAD1 (OAP10523), DcLIP (AAD01804), At2G42690 (818869), LeLID1 (XP_004232963), CaPLA1 (EF595843), AtEDS1 (AEE78366), AtPAD4 (AEE78945), AtSAG101 (NP_568307).

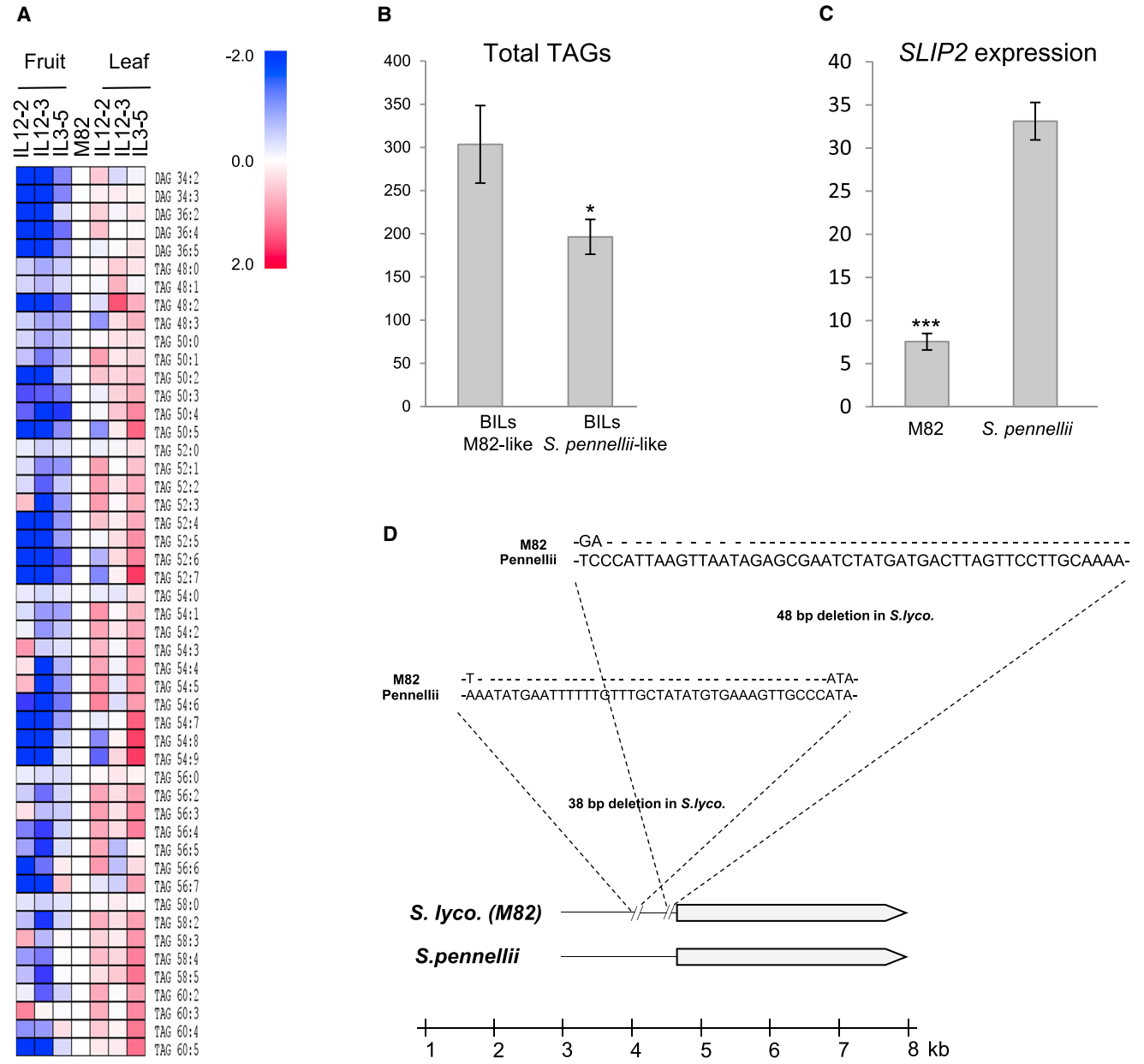

Figure 5. Characterization of the IL3-5 mQTL Harboring the *SLIP2* Gene.

(A) Heatmap showing DAG and TAG levels in fruit and leaf of IL12-2/3 (*SpLIP1*) and IL3-5 (*SpLIP2*). M82 levels are defined as 1 (always white). Decreased levels are marked blue, and increased levels red. The heatmap shows decreased levels of almost all DAGs and TAGs in fruits of the three lines, indicating the exclusive expression of *LIP1* and *2* in fruit and the similarity in their function, while lipid levels in leaf are more variable due to different stochastic factors unrelated to *LIP1* or *2* (which are not expressed there).

(B) Levels of total TAGs in M82-like BILs compared with *S. pennellii*-like BILs. The means of 15 (M82) and 12 (*S. pennellii*) lines are shown. Error bars indicate SE; asterisk indicates significant differences (*$p < 0.05$).

(C) Expression of *LIP1* in M82 and *S. pennellii* fruit. Error bars indicate SE; asterisks indicate significant difference (***$p < 0.001$).

(D) The promoter of the M82 allele of *LIP2* features two deletions compared with the *S. pennellii* allele.

found in M82 (Figure 7B). Moreover, when changes in the lipid profiles were studied at earlier developmental time points, smaller changes were generally observed in the levels of the aforementioned metabolites (Supplemental Table 7), consistent with the expression of *LIP1*. We additionally carried out fatty acid and primary metabolite profiling to analyze the levels of lipase-activity products, namely glycerol and fatty acids. While the levels of glycerol were clearly higher in IL12-3 than M82 and returned to M82 levels following *SpLIP1* silencing (Figure 7B), those of the fatty acids were largely invariant (Supplemental Table 8). This result suggests that red ripe fruit has a limited capacity to further catabolize glycerol, but that the capacity for catabolizing fatty acids is not saturated in IL12-3. Of note, glycerol levels show significant ($p < 0.001$) increase in all four

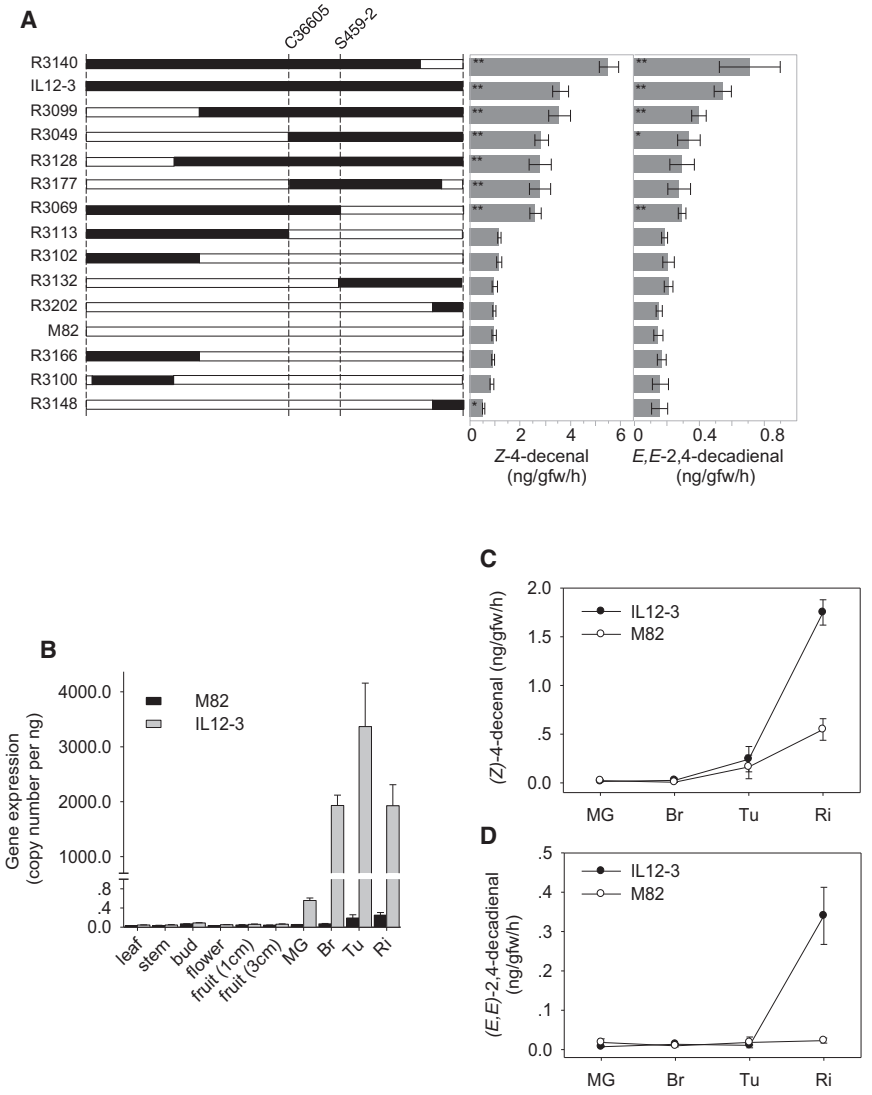

Figure 6. Association of *Z*-4-decenal and *E*,*E*-2,4-decadienal Contents with *LIP1*.

(A) Each F4 generation sub-IL is shown by a combination of black and white rectangles, representing the *S. pennellii* and *S. lycopersicum* genome fragments, respectively. Sub-IL borders were defined with the molecular markers listed in Supplemental Table 1. Emission levels (ng/gfw/h) of *Z*-4-decenal and *E*,*E*-2,4-decadienal in each line are shown (error bars represent SE, $n \geq 4$). VOC levels significantly different from those of M82 are indicated by double asterisks (**$p < 0.01$) and single asterisks (*$p < 0.05$). Linkage of higher contents of *Z*-4-decenal and *E*,*E*-2,4-decadienal with the region defined by molecular markers C1328/C36605 and C202998/S459-2 (harboring the *LIP1* gene) is indicated by dashed lines.

(B) Expression of *Sp/SlLIP1* in different tissues of IL12-3/M82 plants (error bars represent SE, $n = 4$). Six different stages of fruit development were assayed.

(C and D) C10 FA-VOC emissions from different developmental stages of IL12-3/M82 fruits. *Z*-4-decenal **(C)** and *E*,*E*-2,4-decadienal **(D)** were measured (error bars represent SE, $n \geq 2$). Mature green (MG), breaker (Br), turning (Tu), fully ripe (Ri).

independent OE lines in comparison with M82 (Supplemental Figure 6B). Analysis of other primary metabolic changes revealed very few that could potentially be ascribed to *LIP1* (i.e., showed an opposite pattern of change comparing M82 with IL12-3 and IL12-3 with the RNAi and OE lines). Dopamine, γ-aminobutyric acid, galactonate, and glycerol 3-phosphate show different change patterns in red ripe fruit (Supplemental Table 9); however, only the comparative levels of glycerol 3-phosphate in IL12–3 and M82 are consistent with the expression pattern of *LIP1* across ripening (Supplemental Table 9). Thus, when these combined data are considered in the context of the large number of metabolites measured in this study, we can conclude that the effects of manipulating *LIP1* are largely relatively specific and provoke relatively few pleiotropic effects.

In addition, the FA-VOC contents of ripe fruits were measured in transgenic and control lines to determine the impact of the OE and RNAi constructs. Although we did not notice a significant increase in FA-VOC levels in OE lines (Supplemental Table 10), out of 18 FA-VOCs quantified, seven were reduced to near-M82 levels in all four RNAi lines (Figure 7C). These included two C10, two C8, one C7, and two C5 volatiles. The other 11 FA-VOCs, including four C5, five C6, one C7, and one C9, were either unchanged or not significantly altered in every RNAi line (Supplemental Table 10). These results confirm the function of *LIP1* in the production of certain FA-VOCs in tomato fruit.

DISCUSSION

The current study provides a comprehensive analysis of the genetic regulation of lipid metabolism in tomato fruit and leaf. To this end we employed an IL population derived from a cross between the commercial *S. lycopersicum* cv. M82 and the wild *S. pennellii*, already extensively used in various studies. Using genetic mapping with lipid levels as phenotypic traits resulted in identification of more than 160 different lipid species of ten different classes, with a total of 1528 and 428 mQTLs in fruit and leaf, respectively. Although plant lipid metabolism has been extensively studied, even in *Arabidopsis* only 40% of the 700 genes that are putatively annotated as lipid metabolism genes are functionally characterized (Li-Beisson et al., 2013). In tomato and other plant species that number is much smaller. As described in the Introduction, while most mapping studies in tomato have targeted cuticular lipids in fruits and leaves (Yeats et al., 2012; Bolger et al., 2014; Ofner et al., 2016; Fernandez-Moreno et al., 2017), the current study provides genetic evidence for key associations between structural, signaling, and storage lipids, and genes involved in their metabolism in tomato.

We observed that lipid metabolism is genetically regulated on two levels: (i) an intra-class (loci that control lipids from one

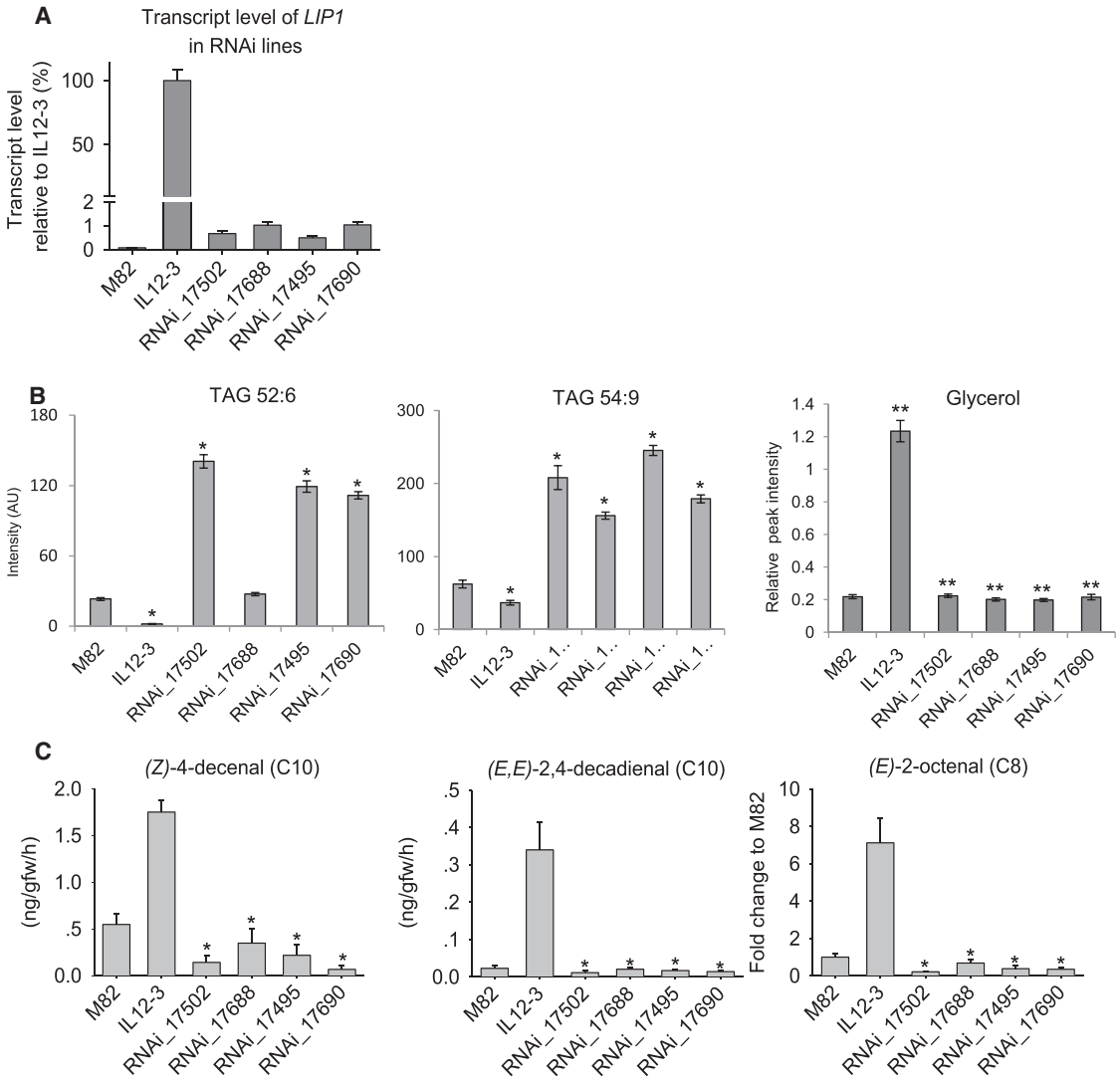

Figure 7. *SpLIP1* Silencing in IL12-3 Plants and Its Effect on Lipid Content and FA-VOC Emissions in Fruit.

(A) Transcript levels of *SpLIP1* in ripe fruits of four silenced transgenic lines relative to IL12-3 and SlLIP1 in M82 (error bars represent SE, $n = 4$).

(B) Levels of triacylglycerol and glycerol accumulating in red ripe fruits of M82, IL12-3, and RNAi lines presented in relative values. Asterisks indicate significant differences (* $p < 0.05$, **$p < 0.001$).

(C) Decreased emissions of FA-VOCs in the fruit of silenced transgenic lines (error bars represent SE, $n \geq 4$). Number of carbons in each VOC is indicated in parentheses. Asterisks indicate significant differences (* $p < 0.05$).

biochemical class, i.e., only lipid species that belong to the TAG lipid class) level; and (ii) an inter-class (loci that control lipids from several classes, i.e., lipids of the lipid classes TAG, PE, and PC) level, suggesting a multilevel genetic-control architecture that is in agreement with the catalytic plasticity of fatty acid modification enzymes in plants (Broun et al., 1998). Synthesis of fatty acid-containing lipids occurs via sequential addition of two-carbon units derived from acetyl-coenzyme A. This is shown in our mapping of biochemically closely related lipids from specific lipid classes to the same locus, reflecting the successive addition of the carbon units conferred by a single enzyme. Prominent examples of this intra-class-level regulation include 43 TAGs that mapped to IL12-3 (Figure 1 and Supplemental Figure 3). Inter-class regulation is exemplified by 12 MGDGs and 13 DGDGs that mapped to IL3-2 in fruit (Figure 1 and Supplemental Figure 3). The DAG moiety has been proposed as the major precursor for TAG synthesis (Bates et al., 2009); hence TAG and DAG were co-mapped to several genomic regions (Figure 1 and Supplemental Figure 3), for instance in IL10-1 (Table 1), carrying a putative diacylglycerol kinase, an enzyme that catalyzes the conversion of DAG to phosphatidic acid.

Significant associations were well distributed across the genome; however, several hotspots could nevertheless be identified, particularly in fruit (Figure 1). Comparison of the mQTLs in both tissues reveals large variation in terms of the lipid species and lipid classes mapped to a specific locus (Figure 1). This result was very different from that found for comparison of QTLs for primary metabolites in various tissues of tomato (Toubiana

et al., 2013) or maize (Wen et al., 2015), suggesting that lipid metabolism, unlike primary metabolism, is regulated in an organ-specific manner. In many cases, the tissue specificity of genetic regulation is also supported by expression QTL (eQTL) data (Table 1); nevertheless, future studies are required for further validation of candidate genes identified in this study. In leaf tissue, the vast majority of detected QTLs were for TAGs, which in the vast majority of instances increased in the ILs (Supplemental Figure 3), with the exception of IL6-2-2 (where they decreased), which shows a necrotic phenotype and was previously reported to contain a 190-kb region influencing defense responses (Sharlach et al., 2013; Ranjan et al., 2016). The higher number of mQTLs in fruit in comparison with leaf may indicate that lipid metabolism genes were less affected in leaf compared with fruit during domestication or it may merely reflect their essentiality in photosynthetic processes, with fruit photosynthesis itself being of only minor importance (Lytovchenko et al., 2011). Indeed, this may well even correspond more broadly to the physiological roles of the two organs, with leaves dedicated to essential, housekeeping tasks such as energy perception, processing, and balance, and fruits occupying (in the context of domestication) secondary, auxiliary roles, especially in terms of lipid roles: appearance, taste, and palatability.

As shown in Figure 2, the overlap between different ILs was helpful in narrowing down the genomic regions of the mQTLs. Furthermore, we performed lipidomic analysis on fruit material from a subset of an additional genetic mapping resource: an experimental population of BILs (Ofner et al., 2016). This population, although only recently released, has already found great utility in narrowing down genomic regions responsible for cuticle (Ofner et al., 2016) and acyl sugar metabolism (Fan et al., 2016), as well as leaf shape (Chitwood et al., 2013) and resistance to the parasite dodder (Krause et al., 2018). The BIL population contains additional copies of introgressed DNA, providing more opportunity for recombination events, thus enabling higher-resolution mapping. This population allowed us to strengthen our mapping results and to narrow down the number of candidate genes in three cases: IL5-3 (Figure 3B and 3C), IL12-3 (Figure 4A), and IL3-5 (Figure 5B). In each case, using BILs resulted in overlapped regions up to two orders of magnitude smaller, in terms of gene number, than the region obtained with mapping using the IL population alone. Specifically for IL12-3, we also generated a sub-IL population that allowed us to narrow down the region further and concomitantly to cross-validate the lipid and volatile results originally observed in IL12-3. The sub-IL bin, containing a gene encoding a putative class III lipase, is correlated with significantly lower levels of DAGs and TAGs and higher levels of C10 volatiles (Figures 4C and 6A). Publicly available RNA-sequencing data indicate that the transcript is present at several thousand-fold higher levels in IL12-3 than in M82. Expression of *SpLIP1* is ripening-associated and correlates with accumulation of C10 volatiles (Figure 6C and 6D). Thus, it seemed a logical candidate for functional validation.

We achieved greater than 95% reduction of *SpLIP1* transcripts in four independent transgenic RNAi lines (Figure 7A). When the relative levels of the individual lipid species were compared, we observed a significant increase in the levels of TAGs when compared with IL12-3 following silencing of *LIP1* (Figure 7B). Moreover, these lines exhibited large reductions in *Z*-4-decenal and *E*,*E*-2,4-decadienal emissions. They also produced significantly lower quantities of C5, C7, and C8 volatiles (Figure 7C), indicating an important role for LIP1 in synthesis of a broad range of fatty acid-derived volatile chemicals correlated with flavor. These results are consistent with those of the OE of orthologs NtOBL1 (Oil body lipase 1) and AtOBL1 from tobacco and *Arabidopsis*, respectively (Muller and Ischebeck, 2018). Primary metabolite analysis revealed that glycerol levels are higher in IL12-3 than M82 and return to M82 levels following silencing of *LIP1* (Figure 7B). Interestingly, the fatty acids (Supplemental Table 8) were largely invariant, suggesting that the red ripe fruit has a limited capacity to further catabolize glycerol but that the capacity for catabolizing the fatty acids is not saturated in IL12-3. In addition, OE of *SpLIP1* in M82 causes decreased levels of TAGs and DAGs and increased level of glycerol (Supplemental Figure 6B), validating the function of LIP1 as a triacylglycerol lipase. In contrast to the RNAi lines, the clear reduction in the levels of most lipid species seen in OE lines of *SpLIP1* (Supplemental Figure 6B and Supplemental Table 7), especially in DAGs and TAGs, was not accompanied by significant increase in FA-VOC levels. This might be explained by the fact that the SpLIP1 enzyme is placed early in the metabolic pathways for FA-VOCs, which might generally cause little effect on the overall rate of the pathway, compared with those enzymes placed close to the end product, which are usually rate limiting. Thus, the flux through the FA-VOC pathway increased by OE of SpLIP1 does not affect the steady-state concentration of pathway products. On the other hand, the absence of change might be attributed to some other effect, such as an increased rate of catabolism of the product (Kinney, 1998).

Although we cannot exclude additional levels of control, our results are consistent with regulation of FA-VOC synthesis in IL12-3 at the level of *LIP1* transcript abundance. In ripening fruit, the *SpLIP1* transcript accumulates to several thousand-fold higher level than its *S. lycopersicum* ortholog. DNA sequencing of the orthologous promoter regions revealed a 1307-bp insertion into the *SlLIP1* gene, moving a tandem repeat of PEREs substantially further away from the translational start site (Supplemental Figure 4B). PERE elements have been shown to confer ethylene-inducible gene expression in *Arabidopsis* (Solano et al., 1998) and tobacco (Kosugi and Ohashi, 2000). The transcriptionally favorable location of these elements in the *SpLIP1* promoter is consistent with relatively high transcript of this gene during climacteric fruit ripening and with considerably lower level of the *SlLIP1* ortholog.

Although the differences in non-C10 volatiles were not consistent in the sub-ILs, analysis of the transgenic plants clearly indicates that the lipase is responsible for generating free fatty acids that produce C5, C6, and C8 volatiles that also contribute to flavor. This result suggests that for some FA-VOCs in IL12-3, other factors such as LOX or HPL become limiting when lipase is overproduced.

Fatty acid-derived volatiles are important contributors to consumer liking of tomato fruits (Tieman et al., 2017). For

example, *Z*-4-decenal is positively correlated with consumer liking and flavor intensity, while *E*,*E*-2,4-decadienal positively correlates with flavor intensity. Similarly, C5–C8 FA-VOCs, namely 1-pentanol, *E*-3-hexen-1-ol, *E*-2-heptenal, and 1-octen-3-one, also make significant contributions to liking and flavor intensity. Although much is known about the roles of LOX (Chen et al., 2004) and HPL (Shen et al., 2014) in the later steps of FA-VOC synthesis, very little is known about the initial step, the release of free fatty acids from glycerol. Moreover, despite the importance of C10 volatiles to flavor, virtually nothing is known about their synthesis. Strikingly, IL3-5 displays similar phenotypic pattern as IL12-3 (Figure 5A) and harbors *LIP2*, the closest homolog of *LIP1* from the seven members of the class III lipase in tomato (Figure 4E). Interestingly, in both cases the mQTLs are supported by eQTLs, with higher expression in *S. pennellii*-derived IL12-3 and IL3-5 in comparison with M82 (Table 1). This might indicate that *LIP2* plays the same role as *LIP1* in TAG degradation.

Taken together, the current work provides comprehensive insights into the genetic regulation of lipid metabolism of tomato fruit pericarp and leaf, elucidating novel lipid–gene associations. Comparison of the mQTLs in both tissues reveals large variation in terms of the lipid species and lipid classes mapped to a specific locus, thus indicating complex modes of regulation in different organs. By utilizing additional genetic mapping resources—BILs and sub-IL populations—we were able to provide additional cross-validation of the candidature of the genomic regions in question and considerably increase mapping resolution. In doing so, we identified a lipase that, when expressed in tomato, has a major effect on production of multiple fatty acid-derived flavor volatiles. The results indicate that levels of some FA-VOCs that are important contributors to flavor may be increased by selecting lines with higher expression of lipase enzyme(s) in fruit. Introgression of the *SpLIP1* allele, in particular into elite tomato varieties, holds the promise of specifically increasing the contents of multiple volatiles that are positively correlated with consumer liking and that lipids, despite their relative low abundance in tomato fruits, are crucial for key agronomical traits in this crop.

METHODS

Plant Material and Growth Conditions

The fruit lipid dataset presented is based on field-grown ILs over two harvests, 2001 and 2003 (Schauer et al., 2006). Plants were grown in the Western Galilee Experimental Station in Akko, Israel, in a completely randomized design with one plant per m^2. Seedlings were grown in greenhouses for 35–40 days and then transferred to the field. The field was irrigated with 320 m^3 of water per 1000 m^3 of field area throughout the season. The harvest of fruit was done when 80%–100% of tomatoes were red (Eshed and Zamir, 1995). Fruit lipid data were also obtained from a BIL population derived from the cross between the cultivated tomato *S. lycopersicum* (CV. M82) and the wild relative *S. pennellii* (LA0716; Ofner et al., 2016), and from sub-IL population generated in this study. Seeds of the reported ILs are available to the research community.

The leaf lipid dataset was obtained from plants grown in the greenhouse in Golm, Germany. In the early March seeds of all 76 *S. pennellii*-derived IL population were sown (Eshed and Zamir, 1995). Seeds were grown for 50 days in a randomized design in a control greenhouse. Plants were top watered. Each IL was planted in at least four replicates with at least one replicate of parental line M82. Mature leaves were harvested at the 50th day of growth and placed into 5-ml tubes and immediately frozen in liquid nitrogen.

Generation of Sub-ILs from IL12-3

S. pennellii introgression line 12-3 (IL12-3) and *S. lycopersicum* (cv M82) were used in this study as parental lines to generate a series of sub-ILs for QTL mapping. A total of 214 F2 plants were derived from a cross between IL12–3 and M82. DNA was extracted from each individual and screened with both the internal and flanking ends of the introgression with markers C20118, C19831, C26157, and C201757 to detect recombination events. This screen resulted in the isolation of 110 recombinant individuals within the interval. Points of recombination within these sub-ILs were further defined by the markers as listed in Supplemental Table 1.Thirteen sub-ILs were selected for propagating homozygous seeds in the F3 generation. Ripe fruits from F4 plants were harvested profiling of lipids and volatiles. Plants were grown in heated greenhouses on the University of Florida campus.

Lipid and Primary Metabolite Extraction Protocol

Metabolites were extracted from ripe fruits and leaf tissues using a protocol described by Hummel et al. (2011). In brief, 120 mg of frozen peeled fruit pericarp (50 mg of leaves) was homogenized using Frosty for 2× 90 s at maximum speed. Metabolites from each aliquot were extracted with 1 ml of pre-cooled (−20°C) extraction buffer (homogenous methanol/methyl-*tert*-butyl-ether [1:3] mixture). After 10 min incubation in 4°C and sonication for 10 min in a sonic bath, 500 μl of water/methanol mixture was added. Samples were then centrifuged (5 min, 14 000 *g*), which led to the formation of two phases: a lipophilic phase and a polar phase. Five hundred microliters of the lipophilic phase and 150 μl of the polar phase were collected and dried under vacuum. The lipophilic phase was resuspended in 200 μl of ASN/isopropanol and used for lipid analysis. The polar phase residue was derivatized for 120 min at 37°C (in 50 ìl of 20 mg ml^{-1} methoxyamine hydrochloride in pyridine) followed by a 30-min treatment at 37°C with 50 ìl of MSTFA and was used for gas chromatography–mass spectrometry (GC–MS) analysis.

Lipid Profiling

Samples were processed using UPLC-FT-MS (Hummel et al., 2011) on a C_8 reverse-phase column (100 × 2.1 mm × 1.7 μm particle size, Waters) at 60°C. The mobile phases consisted of 1% 1 M NH_4OAc and 0.1% acetic acid in water (buffer A) and acetonitrile/isopropanol (7:3, UPLC grade BioSolve) supplemented with 1 M NH_4Ac and 0.1% acetic acid (buffer B). The dried lipid extracts were resuspended in 500 μl of buffer B. The following gradient profile was applied: 1 min 45% A, 3 min linear gradient from 45% A to 35% A, 8 min linear gradient from 25% to 11% A, 3 min linear gradient from 11% to 1% A. Finally, after washing the column for 3 min with 1% A the buffer was set back to 45% A and the column was re-equilibrated for 4 min, leading to a total run time of 22 min. The flow rate of the mobile phase was 400 μl/min.

The mass spectra were acquired using an Exactive mass spectrometer (Thermo Fisher, http://www.thermofisher.com) equipped with an ESI interface. All the spectra were recorded using altering full-scan and all-ion fragmentation scan mode, covering a mass range from 100–1500 *m/z* at a capillary voltage of 3.0 kV, with a sheath gas flow value of 60 and an auxiliary gas flow of 35. The resolution was set to 10 000 with 10 scans per second, restricting the Orbitrap loading time to a maximum of 100 ms with a target value of 1E6 ions. The capillary temperature was set to 150°C, while the drying gas in the heated electrospray source was set to 350°C. The skimmer voltage was held at 25 V while the tube lens was set to a value of 130 V. The spectra were recorded from minute 1 to minute 20 of the UPLC gradients.

Processing of chromatograms, peak detection, and integration were performed using REFINER MS 10.0 (GeneData, http://www.genedata.com) or Xcalibur (Version 3.1, Thermo Fisher, Bremen, Germany). In the first approach the molecular masses, retention time, and associated peak intensities for the three replicates of each sample were extracted from the raw files, which contained the full-scan MS and the all-ion fragmentation MS data. Processing of MS data included the removal of the fragmentation information, isotopic peaks, and chemical noise. Further peak filtering on the manually extracted spectra or the aligned data matrices was performed. Obtained features (*m/z* at a certain retention time) were queried against an in-house lipid database for further annotation. MS/MS fragmentation using collision-induced dissociation mass spectra (25 eV collision energy) was used for further validation of representatives of different lipid classes (Supplemental Figure 2C). The database used in this project includes nearly 200 lipid species of the following classes: diacylglycerols (DAGs), digalactosyldiacylglycerols (DGDGs), monogalactosyldiacylglycerols (MGDGs), phosphatidylcholines (PCs), phosphatidylethanolamines (PEs), phosphatidylglycerols (PGs), phosphatidylserines (PSs), phosphatidylinositols (PIs), sulfoquinovosyl diacylglycerols (SQDGs), and triacylglycerides (TAGs). Metabolomic data have been deposited in the EMBL-EBI MetaboLights database (https://doi.org/10.1093/nar/gks1004. PubMed: 23109552) with the identifier MTBLS693. The complete dataset can be accessed at https://www.ebi.ac.uk/metabolights/MTBLS693.

Primary Metabolite Analysis

The GC–MS system used was a gas chromatograph coupled to a time-of-flight mass spectrometer (Pegasus III, Leco). An autosampler system (PAL) injected the samples. Helium was used as carrier gas at a constant flow rate of 2 ml s^{-1} and gas chromatography was performed on a 30-m DB-35 column. The injection temperature was 230°C and the transfer line and ion source were set to 250°C. The initial temperature of the oven (85°C) increased at a rate of 15°C min^{-1} up to a final temperature of 360°C. After a solvent delay of 180 s mass spectra were recorded at 20 scans s^{-1} with *m/z* 70–600 scanning range. Chromatograms and mass spectra were evaluated by using Chroma TOF 1.0 (Leco) and TagFinder 4.0 software (Roessner et al., 2001; Schauer et al., 2008).

Volatile Collection and Analysis

Plants from each line were grown in the greenhouse in two to three randomized replicates. At least five fruits from each line (fruit from each replicate was combined for each sample collection) were used for volatiles analysis. Fruit was obtained from three weekly harvests. Volatiles were collected from chopped ripe fruit (as well as other growth stages for specific purposes) during a 1-h period as previously described (Tieman et al., 2006a, 2006b). Retention times were compared with known standards and identities of volatile peaks were confirmed by GC–MS (Agilent 5975, www.agilent.com).

Fatty Acid Measurements

For gas chromatography flame ionization detection (GC-FID), 50 mg of materials for the extraction were used by adding 1 ml of 1 N HCl/methanol solution (Sigma-Aldrich). An internal standard (100 μl of FA15:0, pentadecanoic acid) was added to each sample before incubation at 80°C in a water bath for 30 min. After cooling to room temperature, 1 ml of 0.9% NaCl and 1 ml of 100% hexane were added to each vial. Vials were shaken for 5 s and centrifuged for 4 min at 1000 rpm. The upper fatty acid methyl ester (FAME)-containing hexane phase was transferred to a new glass vial, where it was concentrated under a stream of N_2. Finally, FAMEs were dissolved in hexane and filled into GC glass vials. The details of the GC-FID method are as follows: injector temperature of 250°C; helium carrier gas; head pressure 25 cm s^{-1} (11.8 psi); GC column, J&W DB23 (Agilent), 30 m × 0.25 mm × 0.25 μm; detector temperature 250°C; detector gas H_2 40 ml min^{-1}, air 450 ml min^{-1}, He make-up gas 30 ml min^{-1}. FAME peaks were identified by comparing their retention time and equivalent chain length on standard FAME. We used FAME Supelco 37 Component FAME Mix (CRM47885, Sigma-Aldrich) and Supelco PUFA No. 3 from Menhaden Oil (47085-U, Sigma-Aldrich) as standards.

QTL Mapping

Lipidomic data were used for QTL mapping. Each IL was compared (by ANOVA *t*-test, using permissive $p \leq 0.05$ and stringent $p \leq 0.01$ cut-offs) with M82. If it was significantly different from the reference genotype M82, the introgression was considered as harboring a QTL.

Tomato Expression Data

The expression data were obtained from previously described RNA-sequencing analysis (Matas et al., 2011; Chitwood et al., 2013; Koenig et al., 2013; Bolger et al., 2014) and warehoused at the tomato functional genomics database available from http://ted.bti.cornell.edu/.

Sequence and Phylogenetic Analysis

Multiple sequence alignment and homology analysis of the DNA and protein sequences was performed using CLUSTALW (http://www.genome.jp/tools/clustalw/). The phylogenetic tree was built using MEGA5.1 (Tamura et al., 2011). The tree was inferred by using the neighbor-joining statistical method with 1000 bootstrap replicates. The percentage of trees in which the associated taxa clustered together is shown next to the branches. The tree is drawn to scale, with branch lengths measured in the number of substitutions per site.

Transgenic Plants

An RNAi construct were made by assembling an inverted repeat sequence against the 450-bp fragment of *SpLIP1* cDNA, spaced by the intron cloned from vector pKANNIBAL (Wesley et al., 2001). This RNAi cassette was incorporated into the plasmid pHK-OE. Expression of the RNAi cassette was under the control of the figwort mosaic virus (FMV) 35S promoter (Richins et al., 1987), and followed by the *Agrobacterium* nopaline synthase (nos) 3′ terminator. For construction of the overexpression vector, the full-length SpLIP1 coding region was cloned and incorporated into the plasmid pHK-OE in a sense orientation under control of the FMV 35S promoter (Richins et al., 1987), followed by the *Agrobacterium* nos 3′ terminator. The oligonucleotides used for vector construction are listed in Supplemental Table 4. The transgene was introduced into line IL12-3 by the method of McCormick et al. (1986) using kanamycin as a selective agent. Transgenic plants were grown to maturity in heated greenhouses. Collection of volatiles from the transgenic plants and corresponding control (M82 and IL12-3) was performed as described above. Gene expression and volatile analysis was performed on fruits from the T2 generation.

Quantitative PCR

Total RNA was extracted from frozen fruit pericarp tissue with an Isolate II RNA Plant Kit (Bioline), followed by DNase (Promega) treatment to remove any contaminating DNA. mRNA levels were measured by real-time qRT–PCR with a SensiFAST SYBR Hi-ROX One-Step Kit (Bioline) and a GeneAmp 5700 Sequence Detection System (Applied Biosystems). The oligonucleotides used are listed in Supplemental Table 4.

Promoter Analysis

Sp/SlLIP1 promoter analysis was performed on the accessions *S. lycopersicum* (M82) and *S. pennellii* (LA0716). Alignment of the promoter region of *SlLIP1* and *SpLIP1* was performed with CLUSTALW (http://www.genome.jp/tools/clustalw/). Identification of transcription binding site within the promoter region was done with PlantPAN 2.0 (http://plantpan2.itps.ncku.edu.tw/) (Chang et al., 2008; Chow et al., 2016).

ACCESSION NUMBERS

Sequences of Sp/SlLIP1 (Sopen12g024200/Solyc12g055730), Sp/SlLIP2 (Sopen03g041520/Solyc03g123750), Sp/SlLIP3 (Sopen02g035570/Solyc02g090920), Sp/SlLIP4 (Sopen02g035580/Solyc02g090930), Sp/SlLIP5

(Sopen02g035590/Solyc02g090940), Sp/SlLIP6 (Sopen04g032400/Solyc04g078800), and Sp/SlLIP7 (Sopen12g030690/Solyc12g088800) are accessible in the Sol Genomics Network database (Fernandez-Pozo et al., 2015). GenBank accessions or NCBI reference numbers are as follows: At3G14360 (NM_112294.5), RcOBL1 (JQ945176), EgLIP1 (JX556215), AtDAD1 (OAP10523), DcLIP (AAD01804), At2G42690 (818869), LeLID1 (XP_004232963), CaPLA1 (EF595843), AtEDS1 (AEE78366), AtPAD4 (AEE78945), and AtSAG101 (NP_568307).

SUPPLEMENTAL INFORMATION

Supplemental Information is available at *Molecular Plant Online*.

FUNDING

Part of this work was also supported by a grant from the National Science Foundation (IOS-0923312) to H.K. S.A. and A.R.F. acknowledge funding of the PlantaSYST project by the European Union's Horizon 2020 research and innovation program (SGA-CSA nos. 664621 and 739582 under FPA no. 664620). D.Z. was funded by a TOMRES grant (H2020 #727929).

AUTHOR CONTRIBUTIONS

K.G., Z.L., S.A., and D.T. performed experiments, analyzed data, and contributed to the writing of the manuscript. A.K. and M.T. performed experiments. D.Z. and I.O. provided genetic resources used in this study. Y.B., H.J.K., and A.R.F. supervised part of the research and contributed to writing the manuscript.

ACKNOWLEDGMENTS

We thank the Israeli Centers of Research Excellence (i-CORE) program on Plant Adaptation to Changing Environment for supporting the Y.B. lab activity. The authors appreciate Gudrun Wolter and Änne Michaelis for excellent technical assistance. We acknowledge Prof. Lothar Willmitzer for critical and helpful discussion. We thank Dr. Hezi Tenenboim for his kind editorial assistance. No conflict of interest declared.

Received: March 23, 2018
Revised: June 12, 2018
Accepted: June 13, 2018
Published: June 26, 2018

REFERENCES

Alseekh, S., Ofner, I., Pleban, T., Tripodi, P., Di Dato, F., Cammareri, M., Mohammad, A., Grandillo, S., Fernie, A.R., and Zamir, D. (2013). Resolution by recombination: breaking up *Solanum pennellii* introgressions. Trends Plant Sci. **18**:536–538.

Alseekh, S., Tohge, T., Wendenberg, R., Scossa, F., Omranian, N., Li, J., Kleessen, S., Giavalisco, P., Pleban, T., Mueller-Roeber, B., et al. (2015). Identification and mode of inheritance of quantitative trait loci for secondary metabolite abundance in tomato. Plant Cell **27**:485–512.

Alseekh, S., Tong, H., Scossa, F., Brotman, Y., Vigroux, F., Tohge, T., Ofner, I., Zamir, D., Nikoloski, Z., and Fernie, A.R. (2017). Canalization of tomato fruit metabolism. Plant Cell **29**:2753–2765.

Asins, M.J., Villalta, I., Aly, M.M., Olias, R., Alvarez, D.E.M.P., Huertas, R., Li, J., Jaime-Perez, N., Haro, R., Raga, V., et al. (2013). Two closely linked tomato HKT coding genes are positional candidates for the major tomato QTL involved in Na^+/K^+ homeostasis. Plant Cell Environ. **36**:1171–1191.

Bates, P.D., Durrett, T.P., Ohlrogge, J.B., and Pollard, M. (2009). Analysis of acyl fluxes through multiple pathways of triacylglycerol synthesis in developing soybean embryos. Plant Physiol. **150**:55–72.

Bolger, A., Scossa, F., Bolger, M.E., Lanz, C., Maumus, F., Tohge, T., Quesneville, H., Alseekh, S., Sorensen, I., Lichtenstein, G., et al. (2014). The genome of the stress-tolerant wild tomato species *Solanum pennellii*. Nat. Genet. **46**:1034–1038.

Broun, P., Shanklin, J., Whittle, E., and Somerville, C. (1998). Catalytic plasticity of fatty acid modification enzymes underlying chemical diversity of plant lipids. Science **282**:1315–1317.

Causse, M., Duffe, P., Gomez, M.C., Buret, M., Damidaux, R., Zamir, D., Gur, A., Chevalier, C., Lemaire-Chamley, M., and Rothan, C. (2004). A genetic map of candidate genes and QTLs involved in tomato fruit size and composition. J. Exp. Bot. **55**:1671–1685.

Chan, E.K., Rowe, H.C., Corwin, J.A., Joseph, B., and Kliebenstein, D.J. (2011). Combining genome-wide association mapping and transcriptional networks to identify novel genes controlling glucosinolates in Arabidopsis thaliana. PLoS Biol. **9**:e1001125.

Chandra-Shekara, A.C., Venugopal, S.C., Barman, S.R., Kachroo, A., and Kachroo, P. (2007). Plastidial fatty acid levels regulate resistance gene-dependent defense signaling in *Arabidopsis*. Proc. Natl. Acad. Sci. USA **104**:7277–7282.

Chang, W.C., Lee, T.Y., Huang, H.D., Huang, H.Y., and Pan, R.L. (2008). PlantPAN: plant promoter analysis navigator, for identifying combinatorial cis-regulatory elements with distance constraint in plant gene groups. BMC Genomics **9**:561.

Chen, G., Hackett, R., Walker, D., Taylor, A., Lin, Z., and Grierson, D. (2004). Identification of a specific isoform of tomato lipoxygenase (TomloxC) involved in the generation of fatty acid-derived flavor compounds. Plant Physiol. **136**:2641–2651.

Chen, W., Gao, Y., Xie, W., Gong, L., Lu, K., Wang, W., Li, Y., Liu, X., Zhang, H., Dong, H., et al. (2014). Genome-wide association analyses provide genetic and biochemical insights into natural variation in rice metabolism. Nat. Genet. **46**:714–721.

Chitwood, D.H., Kumar, R., Headland, L.R., Ranjan, A., Covington, M.F., Ichihashi, Y., Fulop, D., Jimenez-Gomez, J.M., Peng, J., Maloof, J.N., et al. (2013). A quantitative genetic basis for leaf morphology in a set of precisely defined tomato introgression lines. Plant Cell **25**:2465–2481.

Chow, C.N., Zheng, H.Q., Wu, N.Y., Chien, C.H., Huang, H.D., Lee, T.Y., Chiang-Hsieh, Y.F., Hou, P.F., Yang, T.Y., and Chang, W.C. (2016). PlantPAN 2.0: an update of plant promoter analysis navigator for reconstructing transcriptional regulatory networks in plants. Nucleic Acids Res. **44**:D1154–D1160.

Christensen, S.A., and Kolomiets, M.V. (2011). The lipid language of plant-fungal interactions. Fungal Genet. Biol. **48**:4–14.

Dicke, M., and Baldwin, I.T. (2010). The evolutionary context for herbivore-induced plant volatiles: beyond the 'cry for help'. Trends Plant Sci. **15**:167–175.

Eastmond, P.J. (2004a). Cloning and characterization of the acid lipase from castor beans. J. Biol. Chem. **279**:45540–45545.

Eastmond, P.J. (2004b). Glycerol-insensitive *Arabidopsis* mutants: gli1 seedlings lack glycerol kinase, accumulate glycerol and are more resistant to abiotic stress. Plant J. **37**:617–625.

Eshed, Y., and Zamir, D. (1995). An introgression line population of *Lycopersicon pennellii* in the cultivated tomato enables the identification and fine mapping of yield-associated QTL. Genetics **141**:1147–1162.

Fan, P., Miller, A.M., Schilmiller, A.L., Liu, X., Ofner, I., Jones, A.D., Zamir, D., and Last, R.L. (2016). In vitro reconstruction and analysis of evolutionary variation of the tomato acylsucrose metabolic network. Proc. Natl. Acad. Sci. USA **113**:E239–E248.

Fernandez-Moreno, J.P., Levy-Samoha, D., Malitsky, S., Monforte, A.J., Orzaez, D., Aharoni, A., and Granell, A. (2017). Uncovering

tomato quantitative trait loci and candidate genes for fruit cuticular lipid composition using the *Solanum pennellii* introgression line population. J. Exp. Bot. **68**:2703–2716.

Fernandez-Pozo, N., Menda, N., Edwards, J.D., Saha, S., Tecle, I.Y., Strickler, S.R., Bombarely, A., Fisher-York, T., Pujar, A., Foerster, H., et al. (2015). The Sol Genomics Network (SGN)—from genotype to phenotype to breeding. Nucleic Acids Res. **43**:D1036–D1041.

Frary, A., Nesbitt, T.C., Grandillo, S., Knaap, E., Cong, B., Liu, J., Meller, J., Elber, R., Alpert, K.B., and Tanksley, S.D. (2000). fw2.2: a quantitative trait locus key to the evolution of tomato fruit size. Science **289**:85–88.

Hummel, J., Segu, S., Li, Y., Irgang, S., Jueppner, J., and Giavalisco, P. (2011). Ultra performance liquid chromatography and high resolution mass spectrometry for the analysis of plant lipids. Front. Plant Sci. **2**:54.

Ishiguro, S., Kawai-Oda, A., Ueda, J., Nishida, I., and Okada, K. (2001). The DEFECTIVE IN ANTHER DEHISCIENCE gene encodes a novel phospholipase A1 catalyzing the initial step of jasmonic acid biosynthesis, which synchronizes pollen maturation, anther dehiscence, and flower opening in *Arabidopsis*. Plant Cell **13**:2191–2209.

Jakab, G., Manrique, A., Zimmerli, L., Metraux, J.P., and Mauch-Mani, B. (2003). Molecular characterization of a novel lipase-like pathogen-inducible gene family of *Arabidopsis*. Plant Physiol. **132**:2230–2239.

Kinney, A.J. (1998). Manipulating flux through plant metabolic pathways. Curr. Opin. Plant Biol. **1**:173–178.

Klee, H.J., and Giovannoni, J.J. (2011). Genetics and control of tomato fruit ripening and quality attributes. Annu. Rev. Genet. **45**:41–59.

Kliebenstein, D., Pedersen, D., Barker, B., and Mitchell-Olds, T. (2002). Comparative analysis of quantitative trait loci controlling glucosinolates, myrosinase and insect resistance in *Arabidopsis thaliana*. Genetics **161**:325–332.

Koenig, D., Jimenez-Gomez, J.M., Kimura, S., Fulop, D., Chitwood, D.H., Headland, L.R., Kumar, R., Covington, M.F., Devisetty, U.K., Tat, A.V., et al. (2013). Comparative transcriptomics reveals patterns of selection in domesticated and wild tomato. Proc. Natl. Acad. Sci. USA **110**:E2655–E2662.

Kosugi, S., and Ohashi, Y. (2000). Cloning and DNA-binding properties of a tobacco Ethylene-Insensitive3 (EIN3) homolog. Nucleic Acids Res. **28**:960–967.

Krause, K., Johnsen, H.R., Pielach, A., Lund, L., Fischer, K., and Rose, J.K.C. (2018). Identification of tomato introgression lines with enhanced susceptibility or resistance to infection by parasitic giant dodder (*Cuscuta reflexa*). Physiol. Plant **162**:205–218.

Li-Beisson, Y., Shorrosh, B., Beisson, F., Andersson, M.X., Arondel, V., Bates, P.D., Baud, S., Bird, D., Debono, A., Durrett, T.P., et al. (2013). Acyl-lipid metabolism. Arabidopsis Book **11**:e0161.

Li, H., Peng, Z., Yang, X., Wang, W., Fu, J., Wang, J., Han, Y., Chai, Y., Guo, T., Yang, N., et al. (2013). Genome-wide association study dissects the genetic architecture of oil biosynthesis in maize kernels. Nat. Genet. **45**:43–50.

Ling, H. (2008). Sequence analysis of GDSL lipase gene family in *Arabidopsis thaliana*. Pak. J. Biol. Sci. **11**:763–767.

Lippman, Z.B., Semel, Y., and Zamir, D. (2007). An integrated view of quantitative trait variation using tomato interspecific introgression lines. Curr. Opin. Genet. Dev. **17**:545–552.

Liu, J., Van Eck, J., Cong, B., and Tanksley, S.D. (2002). A new class of regulatory genes underlying the cause of pear-shaped tomato fruit. Proc. Natl. Acad. Sci. USA **99**:13302–13306.

Lytovchenko, A., Eickmeier, I., Pons, C., Osorio, S., Szecowka, M., Lehmberg, K., Arrivault, S., Tohge, T., Pineda, B., Anton, M.T., et al. (2011). Tomato fruit photosynthesis is seemingly unimportant in primary metabolism and ripening but plays a considerable role in seed development. Plant Physiol. **157**:1650–1663.

Mageroy, M.H., Tieman, D.M., Floystad, A., Taylor, M.G., and Klee, H.J. (2012). A Solanum lycopersicum catechol-O-methyltransferase involved in synthesis of the flavor molecule guaiacol. Plant J. **69**:1043–1051.

Manning, K., Tor, M., Poole, M., Hong, Y., Thompson, A.J., King, G.J., Giovannoni, J.J., and Seymour, G.B. (2006). A naturally occurring epigenetic mutation in a gene encoding an SBP-box transcription factor inhibits tomato fruit ripening. Nat. Genet. **38**:948–952.

Martin, G.B., Brommonschenkel, S.H., Chunwongse, J., Frary, A., Ganal, M.W., Spivey, R., Wu, T., Earle, E.D., and Tanksley, S.D. (1993). Map-based cloning of a protein kinase gene conferring disease resistance in tomato. Science **262**:1432–1436.

Matas, A.J., Yeats, T.H., Buda, G.J., Zheng, Y., Chatterjee, S., Tohge, T., Ponnala, L., Adato, A., Aharoni, A., Stark, R., et al. (2011). Tissue- and cell-type specific transcriptome profiling of expanding tomato fruit provides insights into metabolic and regulatory specialization and cuticle formation. Plant Cell **23**:3893–3910.

Mathieu, S., Cin, V.D., Fei, Z., Li, H., Bliss, P., Taylor, M.G., Klee, H.J., and Tieman, D.M. (2009). Flavour compounds in tomato fruits: identification of loci and potential pathways affecting volatile composition. J. Exp. Bot. **60**:325–337.

Matsuda, F., Nakabayashi, R., Yang, Z., Okazaki, Y., Yonemaru, J., Ebana, K., Yano, M., and Saito, K. (2015). Metabolome-genome-wide association study dissects genetic architecture for generating natural variation in rice secondary metabolism. Plant J. **81**:13–23.

Matsui, K., Fukutomi, S., Ishii, M., and Kajiwara, T. (2004). A tomato lipase homologous to DAD1 (LeLID1) is induced in post-germinative growing stage and encodes a triacylglycerol lipase. FEBS Lett. **569**:195–200.

McCormick, S., Niedermeyer, J., Fry, J., Barnason, A., Horsch, R., and Fraley, R. (1986). Leaf disc transformation of cultivated tomato (*L. esculentum*) using *Agrobacterium tumefaciens*. Plant Cell Rep. **5**:81–84.

Minutolo, M., Amalfitano, C., Evidente, A., Frusciante, L., and Errico, A. (2013). Polyphenol distribution in plant organs of tomato introgression lines. Nat. Prod. Res. **27**:787–795.

Mukherjee, K.D. (1994). Plant lipases and their application in lipid biotransformations. Prog. Lipid Res. **33**:165–174.

Muller, A.O., and Ischebeck, T. (2018). Characterization of the enzymatic activity and physiological function of the lipid droplet-associated triacylglycerol lipase AtOBL1. New Phytol. **217**:1062–1076.

Nakamura, Y. (2017). Plant phospholipid diversity: emerging functions in metabolism and protein-lipid interactions. Trends Plant Sci. **22**:1027–1040.

Nurniwalis, A.W., Zubaidah, R., Akmar, A.S.N., Zulkifli, H., Arif, M.A.M., Massawe, F.J., Chan, K.L., and Parveez, G.K.A. (2015). Genomic structure and characterization of a lipase class 3 gene and promoter from oil palm. Biol. Plant. **59**:227–236.

Ofner, I., Lashbrooke, J., Pleban, T., Aharoni, A., and Zamir, D. (2016). *Solanum pennellii* backcross inbred lines (BILs) link small genomic bins with tomato traits. Plant J. **87**:151–160.

Overy, S.A., Walker, H.J., Malone, S., Howard, T.P., Baxter, C.J., Sweetlove, L.J., Hill, S.A., and Quick, W.P. (2005). Application of

metabolite profiling to the identification of traits in a population of tomato introgression lines. J. Exp. Bot. **56**:287–296.

Peralta, I.E., Knapp, S., and Spooner, D.M. (2006). Nomenclature for wild and cultivated tomatoes. Tomato Genetics Cooperative Report **56**:6–12.

Quadrana, L., Almeida, J., Asis, R., Duffy, T., Dominguez, P.G., Bermudez, L., Conti, G., Correa da Silva, J.V., Peralta, I.E., Colot, V., et al. (2014). Natural occurring epialleles determine vitamin E accumulation in tomato fruits. Nat. Commun. **5**:3027.

Rambla, J.L., Medina, A., Fernandez-Del-Carmen, A., Barrantes, W., Grandillo, S., Cammareri, M., Lopez-Casado, G., Rodrigo, G., Alonso, A., Garcia-Martinez, S., et al. (2017). Identification, introgression, and validation of fruit volatile QTLs from a red-fruited wild tomato species. J. Exp. Bot. **68**:429–442.

Rambla, J.L., Tikunov, Y.M., Monforte, A.J., Bovy, A.G., and Granell, A. (2014). The expanded tomato fruit volatile landscape. J. Exp. Bot. **65**:4613–4623.

Ranjan, A., Budke, J.M., Rowland, S.D., Chitwood, D.H., Kumar, R., Carriedo, L., Ichihashi, Y., Zumstein, K., Maloof, J.N., and Sinha, N.R. (2016). eQTL regulating transcript levels associated with diverse biological processes in tomato. Plant Physiol. **172**:328–340.

Richins, R.D., Scholthof, H.B., and Shepherd, R.J. (1987). Sequence of figwort mosaic virus DNA (caulimovirus group). Nucleic Acids Res. **15**:8451–8466.

Roessner, U., Luedemann, A., Brust, D., Fiehn, O., Linke, T., Willmitzer, L., and Fernie, A. (2001). Metabolic profiling allows comprehensive phenotyping of genetically or environmentally modified plant systems. Plant Cell **13**:11–29.

Ronen, G., Carmel-Goren, L., Zamir, D., and Hirschberg, J. (2000). An alternative pathway to beta -carotene formation in plant chromoplasts discovered by map-based cloning of beta and old-gold color mutations in tomato. Proc. Natl. Acad. Sci. USA **97**:11102–11107.

Rousseaux, M.C., Jones, C.M., Adams, D., Chetelat, R., Bennett, A., and Powell, A. (2005). QTL analysis of fruit antioxidants in tomato using *Lycopersicon pennellii* introgression lines. Theor. Appl. Genet. **111**:1396–1408.

Scala, A., Allmann, S., Mirabella, R., Haring, M.A., and Schuurink, R.C. (2013). Green leaf volatiles: a plant's multifunctional weapon against herbivores and pathogens. Int. J. Mol. Sci. **14**:17781–17811.

Schauer, N., Semel, Y., Balbo, I., Steinfath, M., Repsilber, D., Selbig, J., Pleban, T., Zamir, D., and Fernie, A.R. (2008). Mode of inheritance of primary metabolic traits in tomato. Plant Cell **20**:509–523.

Schauer, N., Semel, Y., Roessner, U., Gur, A., Balbo, I., Carrari, F., Pleban, T., Perez-Melis, A., Bruedigam, C., Kopka, J., et al. (2006). Comprehensive metabolic profiling and phenotyping of interspecific introgression lines for tomato improvement. Nat. Biotechnol. **24**:447–454.

Schilmiller, A.L., Gilgallon, K., Ghosh, B., Jones, A.D., and Last, R.L. (2016). Acylsugar acylhydrolases: carboxylesterase-catalyzed hydrolysis of acylsugars in tomato trichomes. Plant Physiol. **170**:1331–1344.

Schilmiller, A.L., Moghe, G.D., Fan, P., Ghosh, B., Ning, J., Jones, A.D., and Last, R.L. (2015). Functionally divergent alleles and duplicated Loci encoding an acyltransferase contribute to acylsugar metabolite diversity in Solanum trichomes. Plant Cell **27**:1002–1017.

Schwab, W., Davidovich-Rikanati, R., and Lewinsohn, E. (2008). Biosynthesis of plant-derived flavor compounds. Plant J. **54**:712–732.

Sharlach, M., Dahlbeck, D., Liu, L., Chiu, J., Jimenez-Gomez, J.M., Kimura, S., Koenig, D., Maloof, J.N., Sinha, N., Minsavage, G.V., et al. (2013). Fine genetic mapping of RXopJ4, a bacterial spot disease resistance locus from *Solanum pennellii* LA716. Theor. Appl. Genet. **126**:601–609.

Shen, J., Tieman, D., Jones, J.B., Taylor, M.G., Schmelz, E., Huffaker, A., Bies, D., Chen, K., and Klee, H.J. (2014). A 13-lipoxygenase, TomloxC, is essential for synthesis of C5 flavour volatiles in tomato. J. Exp. Bot. **65**:419–428.

Solano, R., Stepanova, A., Chao, Q., and Ecker, J.R. (1998). Nuclear events in ethylene signaling: a transcriptional cascade mediated by ETHYLENE-INSENSITIVE3 and ETHYLENE-RESPONSE-FACTOR1. Genes Dev. **12**:3703–3714.

Tamura, K., Peterson, D., Peterson, N., Stecher, G., Nei, M., and Kumar, S. (2011). MEGA5: molecular evolutionary genetics analysis using maximum likelihood, evolutionary distance, and maximum parsimony methods. Mol Biol Evol. **28**:2731–2739.

Tenenboim, H., and Brotman, Y. (2016). Omic relief for the biotically stressed: metabolomics of plant biotic interactions. Trends Plant Sci. **21**:781–791.

Tieman, D., Taylor, M., Schauer, N., Fernie, A.R., Hanson, A.D., and Klee, H.J. (2006a). Tomato aromatic amino acid decarboxylases participate in synthesis of the flavor volatiles 2-phenylethanol and 2-phenylacetaldehyde. Proc. Natl. Acad. Sci. USA **103**:8287–8292.

Tieman, D.M., Zeigler, M., Schmelz, E.A., Taylor, M.G., Bliss, P., Kirst, M., and Klee, H.J. (2006b). Identification of loci affecting flavour volatile emissions in tomato fruits. J. Exp. Bot. **57**:887–896.

Tieman, D., Zhu, G., Resende, M.F., Jr., Lin, T., Nguyen, C., Bies, D., Rambla, J.L., Beltran, K.S., Taylor, M., Zhang, B., et al. (2017). A chemical genetic roadmap to improved tomato flavor. Science **355**:391–394.

Tomato Genome Consortium. (2012). The tomato genome sequence provides insights into fleshy fruit evolution. Nature. **485**:635–641.

Toubiana, D., Batushansky, A., Tzfadia, O., Scossa, F., Khan, A., Barak, S., Zamir, D., Fernie, A.R., Nikoloski, Z., and Fait, A. (2015). Combined correlation-based network and mQTL analyses efficiently identified loci for branched-chain amino acid, serine to threonine, and proline metabolism in tomato seeds. Plant J. **81**:121–133.

Toubiana, D., Fernie, A.R., Nikoloski, Z., and Fait, A. (2013). Network analysis: tackling complex data to study plant metabolism. Trends Biotechnol. **31**:29–36.

Toubiana, D., Semel, Y., Tohge, T., Beleggia, R., Cattivelli, L., Rosental, L., Nikoloski, Z., Zamir, D., Fernie, A.R., and Fait, A. (2012). Metabolic profiling of a mapping population exposes new insights in the regulation of seed metabolism and seed, fruit, and plant relations. PLoS Genet. **8**:e1002612.

Vancanneyt, G., Sanz, C., Farmaki, T., Paneque, M., Ortego, F., Castanera, P., and Sanchez-Serrano, J.J. (2001). Hydroperoxide lyase depletion in transgenic potato plants leads to an increase in aphid performance. Proc. Natl. Acad. Sci. USA **98**:8139–8144.

Vick, B.A., and Zimmerman, D.C. (1984). Biosynthesis of jasmonic acid by several plant species. Plant Physiol. **75**:458–461.

Wang, C., Xing, J., Chin, C.K., Ho, C.T., and Martin, C.E. (2001). Modification of fatty acids changes the flavor volatiles in tomato leaves. Phytochemistry **58**:227–232.

Weber, H. (2002). Fatty acid-derived signals in plants. Trends Plant Sci. **7**:217–224.

Wen, W., Li, K., Alseekh, S., Omranian, N., Zhao, L., Zhou, Y., Xiao, Y., Jin, M., Yang, N., Liu, H., et al. (2015). Genetic determinants of the network of primary metabolism and their relationships to plant performance in a maize recombinant inbred line population. Plant Cell **27**:1839–1856.

Wesley, S.V., Helliwell, C.A., Smith, N.A., Wang, M.B., Rouse, D.T., Liu, Q., Gooding, P.S., Singh, S.P., Abbott, D., Stoutjesdijk, P.A., et al. (2001). Construct design for efficient, effective and high-throughput gene silencing in plants. Plant J. **27**:581–590.

Wu, S., Tohge, T., Cuadros-Inostroza, A., Tong, H., Tenenboim, H., Kooke, R., Meret, M., Keurentjes, J.B., Nikoloski, Z., Fernie, A.R., et al. (2018). Mapping the *Arabidopsis* metabolic landscape by untargeted metabolomics at different environmental conditions. Mol. Plant **11**:118–134.

Xiao, H., Jiang, N., Schaffner, E., Stockinger, E.J., and van der Knaap, E. (2008). A retrotransposon-mediated gene duplication underlies morphological variation of tomato fruit. Science **319**: 1527–1530.

Yeats, T.H., Buda, G.J., Wang, Z., Chehanovsky, N., Moyle, L.C., Jetter, R., Schaffer, A.A., and Rose, J.K. (2012). The fruit cuticles of wild tomato species exhibit architectural and chemical diversity, providing a new model for studying the evolution of cuticle function. Plant J. **69**:655–666.